Green Chemistry

ROYAL SOCIETY OF CHEMISTRY

CRITICAL REVIEW

View Article Online
View Journal | View Issue

Check for updates

Cite this: *Green Chem.*, 2024, **26**, 3546

Homogeneous *vs.* heterogeneous catalysts for acceptorless dehydrogenation of biomass-derived glycerol and ethanol towards circular chemistry

Kai Wang, Jonathan Horlyck, Nan An and Adelina Voutchkova-Kostal *

Received 12th November 2023,
Accepted 5th February 2024

DOI: 10.1039/d3gc04378a

rsc.li/greenchem

The benefits of transitioning to chemical and material circularity are readily apparent. However, identifying and developing the necessary chemical transformations for platform chemical recycling is a significant challenge. Alcohols are an important industrial platform class owing to existing demand and the potential for their renewable supply through the utilization of biomass processing waste streams. Acceptorless Dehydrogenation (AD) is a critical process in the context of circularity, particularly in the transformation of alcohols. This mini-review offers an in-depth examination of both homogeneous and heterogeneous catalytic processes used in acceptorless dehydrogenation. We primarily concentrate on two sustainable feedstocks, glycerol and ethanol. Through the assessment and juxtaposition of homogenous and heterogeneous catalysts in the context of the alcoholysis of glycerol and ethanol, we aim to establish a comparison based on activity, longevity, and the green chemistry metrics associated with the catalytic processes (specifically the *E*-factor; energy economy coefficient, ε; and environmental energy impact factor, ξ). We established evaluation criteria using the matrics to provide a means for comparison among homogeneous and heterogeneous catalysts and help identify promising catalyst classes that can be further developed. This review seeks to shed light on the existing constraints that must be addressed to advance the development of catalysts that are more efficient, cost-effective, and resilient for AD reactions.

1. Introduction

The use of catalysis plays a crucial role in the advancement of circular chemical processes, as it enables the enhancement of low-value waste streams and the establishment of novel approaches to chemical manufacturing that are based on reversible reactions. While the former approach focuses on implementing short-term measures to enhance circularity by closing the loop on chemicals already in use, the latter approach offers more robust methods to drive innovation in chemistry and achieve a competitive edge. Therefore, the development of catalytic processes that facilitate the implementation of a circular economy for chemicals is a complex and ongoing undertaking that necessitates collaborative efforts from the catalysis communities in the fields of chemistry and engineering.

In the short-term, we seek opportunities to apply existing catalytic processes to the valorization of waste streams. While there are numerous such waste streams worthy of pursuit, alcohols and polyols offer a relatively accessible entry-point. Alcohols and polyols derived from biomass processing, from industrial waste (*e.g.* from furniture manufacturing, painting and leather processing)[1] and from Fischer–Tropsch processes[2] are abundant and available at low cost. Their low hazard and high biodegradability further enhance their appeal as platform chemicals. Among the C1–C4 alcohols from renewable sources, glycerol, ethanol, butanol and polyols derived from sugars are highly promising for valorization.[3] Numerous catalytic processes have been reported for valorization of these renewable sources with both homogeneous and heterogeneous catalysts. Most of them start with alcohol dehydrogenation as their initial step, though these processes may be highly distinct. While an exhaustive review of the acceptorless dehydrogenation processes for all alcohols would be prohibitively extensive, we focus here on two representative substrates – glycerol, as a polyol, and ethanol, as a primary alcohol. The choice of these model substrates is also guided by the abundant industrial applications of both.

Dehydrogenation is thermodynamically and kinetically challenging and thus significantly less developed than hydrogenation. However, it is a powerful tool for generating both hydrogen gas (hydrogen storage applications) (Fig. 1a) and reactive unsaturated intermediates that can undergo functionalization and controlled breakdown (Fig. 1b). For

Department of Chemistry, The George Washington University, 800 22nd St. NW, Washington, DC 20052, USA. E-mail: avoutchkova@gwu.edu

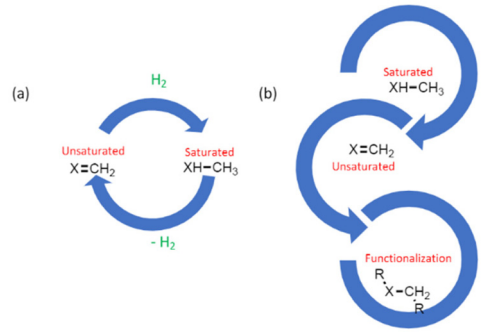

Fig. 1 (a) Cycling between saturated and unsaturated substrates, (b) employing dehydrogenation for potential functionalization.

example, introducing unsaturation *via* the dehydrogenation of C–C and C–X bonds (where X = NR_2, OH, SH, *etc.*) can be followed by functionalization to afford a higher-value chemical, and the reverse (elimination) back to the unsaturated analog to complete circularity. Dehydrogenation is thus a highly useful transformation that is pivotal in both organic synthesis and chemical industry. The most atom-economical form of dehydrogenation is acceptorless dehydrogenation (AD), which requires no oxidant or additives and produces only H_2.[4,5] The liberated H_2 from AD can be employed in hydrogen storage system or be consumed *in situ* to hydrogenate the unsaturated intermediates.

Traditionally, homogeneous catalysts have been developed for alcohol dehydrogenation, such that they are chemoselective and active under relatively mild conditions. Recently, however, it has been demonstrated that an expanding number of heterogeneous catalysts are competitive with their homogeneous counterparts in terms of activity and selectivity. The objective of this review is to establish a comprehensive and methodical comparison of both types of catalysts utilized in acceptorless dehydrogenation of ethanol and glycerol. As a result, we emphasize the distinct benefits attained by each category of catalysts, as well as the deficiencies that necessitate attention as we strive to develop catalysts that are more cost-effective, resilient, and efficient. Furthermore, we strive to underscore the difficulties that arise when it comes to formulating catalysts in a way that adheres to the tenets of green chemistry and utilizing suitable metrics to assess the effects of circular processes.[6]

The metrics applied to the processes here include *E* factor, energy economy coefficient (ε) and environmental energy impact factor (ξ). Subsequent to the original proposal of atom economy as a useful metric of inherent material efficiency in chemical transformations by Trost,[145] reports have highlighted the inherent limitations and potential applications of this simple metric.[145,146] As a result, additional metrics were proposed to capture the effect of solvents, additives, and catalysts on material efficiency.[146–149] While the research development on the latter metrics has progressed, it is clear that universal metrics will need to be modified for specific types of transformations to make them most informative for comparison, as highlighted in the most recent review on the subject.[150]

$$E\,\text{factor} = \frac{\text{Waste (kg)}}{\text{Product (kg)}} \quad (1)$$

E factor calculation assumes waste is composed of unreacted alcohol, solvents, additives, and homogenous catalysts. Heterogeneous catalysts are not included, as they can theoretically be reused. Energy economy coefficient (ε), recently defined by Thielemans *et al.*[7] is calculated as follows,

$$\varepsilon = \frac{Y}{T \times t} \quad (2)$$

where *Y* is the yield in mass fraction, *T* is the reaction temperature (degrees Celsius), and *t* is the reaction time (in minutes). The latter metric only considers heating of the reaction, and not solvent distillation. Finally, the ratio of *E* factor and Energy economy coefficient provides another useful metric, designated as Environmental Energy Impact Factor (ξ),[7] reflecting a balanced view of waste to energy consumption.

$$\xi = \frac{E\,\text{factor}}{\varepsilon} \quad (3)$$

We note that the latter simple process metrics only capture material and energy efficiency, and do not constitute comprehensive lifecycle or technoeconomic analyses needed to assess environmental and economic viability of a new technology at-scale. LCA and TEA are also highly involving analyses, requiring numerous inputs that are only available, including energy source, raw material sources, plant location and specific infrastructure have been identified. However, the latter metrics employed here can be a helpful first step in identifying promising catalytic methods that are have potential to lead to development of "greener" processes when scaled.

2. Glycerol dehydrogenation processes

Biodiesel production from crops has increased dramatically over the past few decades; global production surpassed 1.5 million tons in 2011 and continues to rise. The principal byproduct, glycerol, comprises less than 10 weight percent of the biodiesel produced.[8] Glycerol is an excellent feedstock due to its eco-friendliness, biodegradability, and low cost. This has fueled research into new valorization processes, such as conversion to propane diols,[9] glyceric acid,[10] cyclic acetals[11] and acrolein.[12] One particularly attractive value-added product of glycerol is lactic acid – a versatile platform chemical with applications in food processing, cosmetics, pharmaceuticals, fine chemical synthesis, and polylactic acid (PLA) synthesis.[13] Use of PLA is growing rapidly due to the shift towards biodegradable and renewable alternatives to petrochemical-derived plastics. Compared to the traditional fermentation process for producing lactic acid, the production of lactic acid

from glycerol is likely to generate less waste while being atom-economical and utilizing a low-value feedstock.

Siebenhofer *et al.* proposed a valorization scheme of glycerol to value-added products by electrochemical oxidation in 2010.[14] The conversion of glycerol to lactic acid proceeds through a dehydrogenation step to form a dihydroxyacetone (DHA) and glyceraldehyde mixture. The latter dehydrates to pyruvaldehyde (PA) and undergoes an intramolecular Cannizzaro reaction to afford lactic acid (Scheme 1).

The main side product, 1,2-PDO, can result from either transfer hydrogenolysis of glycerol (*via* dehydration/hydrogenation), or from transfer hydrogenation of glyceraldehyde (GA). The relative rates of dehydration *vs.* dehydrogenation affect the selectivity for 1,2-PDO *vs.* LAC. Hydrogenation of LAC to 1,2-PDO has been excluded as a possibility, as is expected based on the high thermodynamic stability of LAC compared to other products.[15] Additional minor products can be formed from GA *via* retro–aldol reactions or decarbonylation to give formic acid (FA) and glycolaldehyde (GLA); the latter can be hydrogenated to methanol and ethylene glycol (EG), respectively.

2.1 Homogeneous catalysts for glycerol dehydrogenation to lactic acid

Several homogeneous catalysts have been reported for glycerol dehydrogenation since the initial report by Siebenhofer *et al.*,[14] which are compared in Fig. 2. The most active reported to-date are based on N-heterocyclic carbene (NHC) complexes of iridium. Crabtree *et al.*[16] first reported a series of iridium(I) and(III) NHC complexes that facilitate the reaction in the presence of stoichiometric hydroxide base. The most active of these was a robust iridium(I) bis(NHC) bis-carbonyl complex (**1**, Fig. 2), which affords on average 337 turnovers per hour at 115 °C and 31 000 TON in 90 h with high selectivity for LAC.[16]

Inspired by the architecture of these catalysts, several groups reported new complexes with improved catalytic activity for this process. Williams *et al.* identified that a bidentate

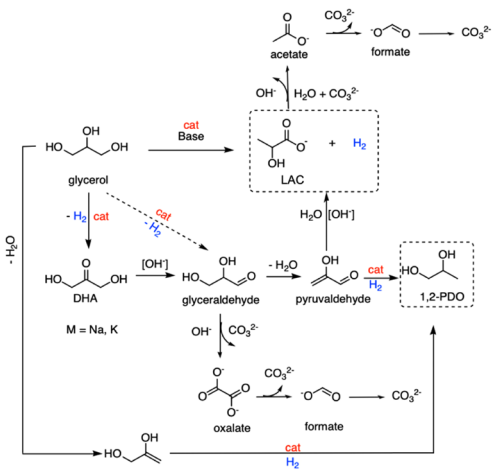

Scheme 1 Glycerol dehydrogenation route *via* DHA/glyceraldehyde.

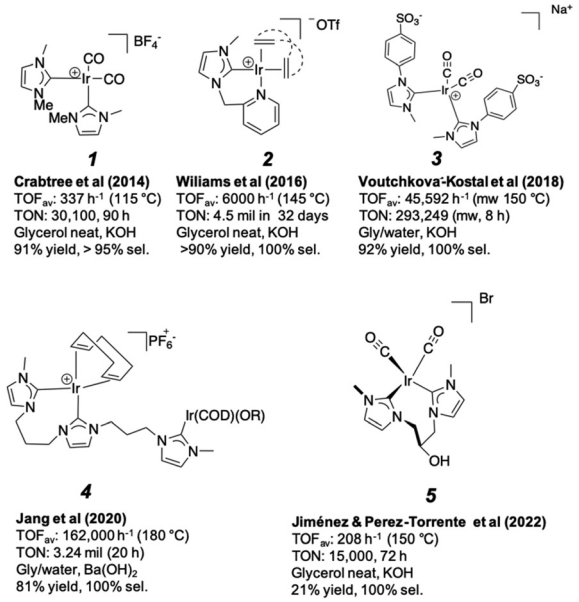

Fig. 2 Iridium homogeneous catalysts for glycerol dehydrogenation and conversion to lactic acid. TOF$_{av}$: average turnover frequency.

(pyridyl)methylcarbene iridium(I) complex (**2**, Fig. 2) to be highly prolific and robust due to the inhibition of catalyst deactivation *via* dimerization, afforded by the chelating (pyridyl) methylcarbene ligand.[17] The latter also makes a charge-neutral complex, which facilitates the cooperative cleavage of the glycerol O–H bond, rather than simple proton transfer. In neat glycerol, **2** affords complete selectivity for LAC with 6000 h^{-1} TOF at 145 °C.

One of the challenges of the homogeneous reactions is the high viscosity of pure glycerol. Dilution with water increases the solubility of the hydroxide base and reduces the viscosity of the reaction mixture, thus increasing mass transfer. However, aqueous media also reduce catalyst solubility. In an attempt to overcome this challenge, we reported a series of water-soluble iridium complexes bearing sulfonate-functionalized NHC ligands.[18] The most active of these was Ir(NHCphSO$_3$)$_2$(CO) complex (**3**), which afforded a TOF 3477 h^{-1} at 150 °C and 1.8 ppm Ir with conventional heating, and 45 592 h^{-1} with microwave heating.

Most recently, Jang *et al.*[19] described a highly efficient bimetallic iridium catalyst (**4**) consisting of triscarbene ligands. The efficiency of the catalysts (TOF of 162 000 h^{-1} with 0.09 ppm Ir at 180 °C) was speculated to be due to the potential cooperativity of two iridium centers. The authors also identified that Ba(OH)$_2$ afforded higher activity than other hydroxide bases examined, including KOH. Comparison of the efficiency of the catalysts in Fig. 2 is, however, challenging due to the differences in reaction temperature, mode of heating (conventional *vs.* microwave), medium composition (neat *vs.* aqueous glycerol) and base used. Furthermore, the reaction rate is highly sensitive to temperature, emphasizing that these parameters must be well-controlled in making conclusions

about the structure–activity relationships revealed by these examples. Jiménez & Perez-Torrente *et al.*[20] synthesized series of Ir(I) complexes featuring bridge-functionalized bis-NHC ligands, which have shown to be robust catalysts for dehydrogenation process of glycerol to LAC with dihydrogen release. When used in an open system with low catalyst loadings and KOH as a base, these catalysts achieved high levels of activity and selectivity towards LAC. The hydroxy-functionalized bis-NHC catalysts were significantly more active than the carboxylate-functionalized catalysts or the unbridged bis-NHC Ir(I) catalyst with hydroxyalkyl-functionalized NHC ligands, and carbonyl complexes demonstrate greater activity than their cyclooctadiene (cod) counterparts. The $[Ir(CO)_2[(MeImCH_2)_2CHOH]]Br$ catalyst (**5**) demonstrated TON for LAC of up to 15 000 at low catalyst loadings.

A generally accepted glycerol dehydrogenation mechanism involving iridium catalysts is presented in Scheme 2. For complexes with labile *cod* ligands, such as **2** and **4**, initial *cod* dissociation is followed by coordination and deprotonation of glycerol, likely to the 2-hydroxy. Subsequent β-hydride elimination forms the iridium hydride and dihydroxyacetone (DHA). The Ir–H can be protonated internally by the hydroxy of dihydroxyacetone, or externally by glycerol or water, liberating H_2. The displacement of DHA by glycerol completes the catalytic cycle. DHA can be isomerized to form glyceraldehyde, which is converted to lactate under basic Cannizzaro conditions. Neither DHA nor glyceraldehyde have been observed under basic conditions, likely because they quickly undergo dehydration and intramolecular Cannizzaro reaction.

A similar mechanism involving β-hydride elimination from the Ir-alkoxide and hydride abstraction using H^+ to release H_2 was proposed by Xiao *et al.* for alcohol dehydrogenation using Ir(III) complexes.[151] However, complexes without labile ligands, such as biscarbonyl Ir(I) carbenes **1**, **3**, and **5**, a different

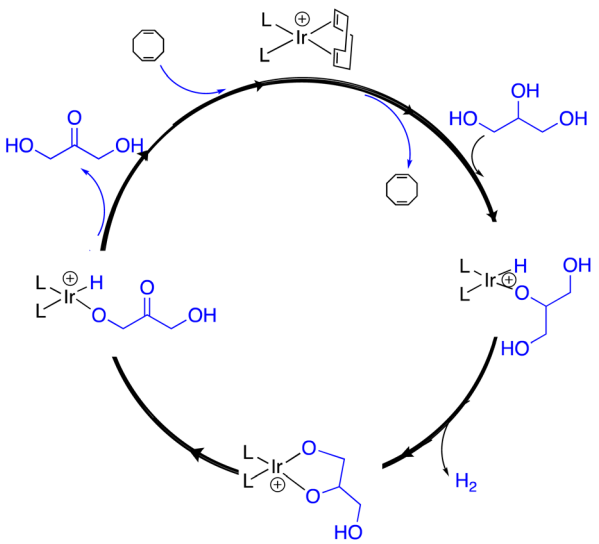

Scheme 2 Proposed catalytic cycle for glycerol dehydrogenation by catalysts **2** and **4** (see Fig. 2), which bear labile ligands.

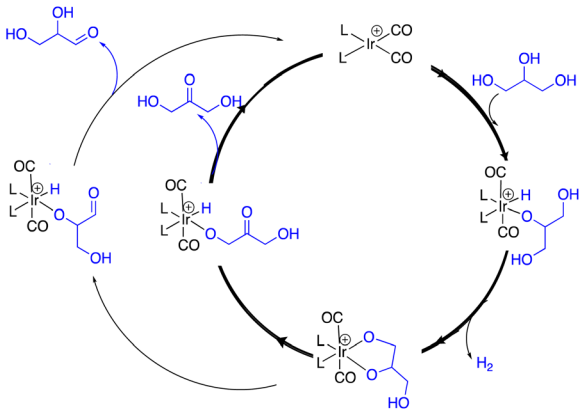

Scheme 3 Proposed catalytic cycle for glycerol dehydrogenation by catalysts **1**, **3** and **5** (see Fig. 2), which lack labile ligands.

mechanism is likely involved. Given that CO substitution in Ir(I) complexes is not facile,[152] we proposed an alternative catalytic cycle, as depicted in Scheme 3. The 16-electron Ir(I) species can undergo O–H oxidative addition with glycerol to form an alkoxy hydride complex,[153] which can eliminate H_2 *via* σ-bond metathesis with an adjacent hydroxyl of glycerol.[154] The chelating bis-alkoxy complex can β-hydride eliminate at the primary or secondary position, releasing glyceraldehyde or DHA *via* O–H reductive elimination.

Beller *et al.* first reported the Ru phosphine (PNP) pincer complex (**6**, Fig. 3), which reaches a TOF of 11 055 h^{-1} with moderate selectivity for lactic acid (67%) at 140 °C.[21] The proposed mechanism for the Ru-catalyzed process is analogous to that for Ir(I) catalysts with labile ligands (Scheme 2), with H2 elimination likely occurring *via* σ-bond metathesis of the glycerol hydroxyl. In 2020, Srivastava & Kumar *et al.*[22] reported

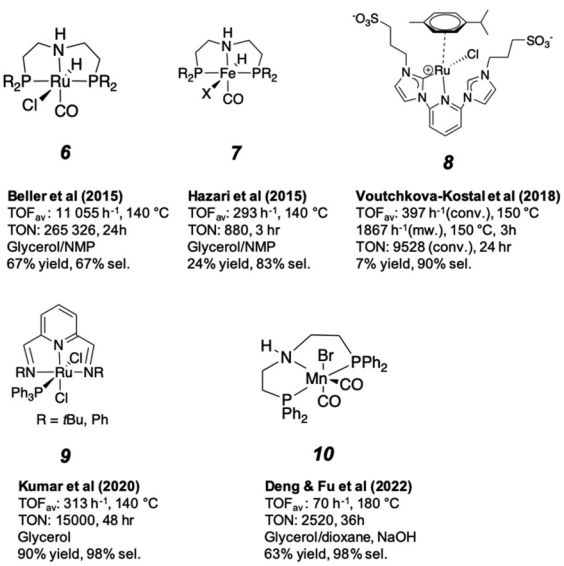

Fig. 3 Ruthenium, iron and manganese homogeneous catalysts for glycerol dehydrogenation and conversion to lactic acid.

the production of lactic acid using NNN-pincer Ru complex (**9**), which affords lower TOF of 313 h^{-1}. The latter also produced ethylene glycol and formic acid, suggesting undesired decarbonylation was occurring. A similar TOF was afforded by NHC complex **8**,[18] in which there is potential for *in situ* formation of a potentially more active CNC Ru complex upon displacement of the *p*-cymene ligand. Although the activity of complex **6** offers promise that further optimization of the ligand architecture could yield more active Ru catalysts, the lower selectivity generally observed with Ru *vs.* Ir complexes may point to relatively lower energy paths to undesired C–C cleavage products, which may be challenging to overcome.

In the only Fe complex reported to-date, Hazari and Crabtree utilized a PNP ligand analogous to that used by Beller *et al.* to synthesize iron complex **7**, which averages 293 turnovers per hour using NMP as co-solvent.[23] This complex provides a direct comparison between the activity of the two metals with the same ligand architectures, and tested under comparable condition.

Most recently, Deng and Fu[24] utilized a pincer Mn complex supported by PNP ligands for the conversion of glycerol to sodium lactate with liberation of dihydrogen, and yielded sodium lactate in 96% yield with 96% selectivity under mild reaction conditions. The complex **10** showed good reactivity and excellent selectivity (up to 98%) being achieved even at low catalyst loadings (0.025 mol%) at 180 °C in 36 hours. Mechanistic studies indicated that the manganese catalyst was primarily responsible for glycerol dehydrogenation, while the amount of sodium hydroxide had a critical impact on the subsequent Cannizzaro reaction.

Evaluating the viability of the aforementioned homogeneous processes for possible implementation in industry presents several obstacles. First, is that process selectivity can be difficult to assess because accurately quantitating conversion of glycerol is challenging by nuclear magnetic resonance spectroscopy (NMR) and necessitates use of high-performance liquid chromatography (HPLC) with a refractive Index (RI) detector. Numerous reports consequently lack glycerol conversion data. Observed glycerol byproducts consist of ethylene glycol, 1,2-PDO, 1,3-PDO, formic acid, and glycerol etherification products. The quantification and discussion of these byproducts is warranted in subsequent reports. Additionally, only a limited number of catalysts have demonstrated efficacy when applied to crude glycerol, which contains numerous impurities such as water and ethanol. Considering the formidable difficulty associated with purifying crude glycerol produced during biodiesel synthesis, the ultimate objective is to utilize the catalysts under consideration for this purpose. Merely catalysts **3** and **6** have demonstrated efficacy when applied to crude glycerol.

2.2 Heterogeneous catalysts in glycerol dehydrogenation to lactic acid

Despite the highly prolific and robust nature of the homogeneous complexes developed to-date for this process, the use of expensive organometallic complexes that cannot be readily recycled calls for development of cheap and robust heterogeneous alternatives, albeit at a trade-off in activity. Such catalysts should also be usable under continuous flow modes, which is highly desirable for process intensification.

Some of the early examples of heterogeneous catalysts for glycerol dehydrogenation relied on oxygen as the hydrogen acceptor, producing water. A few of these examples include Au/CeO_2,[25] Au–Pt@CeO_2,[26] Au–Pt@TiO_2,[27] Pt/C,[28–30] Pt/L-Nb_2O_5,[31] Pt/PVP[32] and Pt/TiO_2 [33] and Ag-phosphomolybdic acid catalysts.[34] A major advantage of many of these, including Pt/TiO_2, Pt/layered-Nb_2O_5 and Pt/PVP, is the ability to facilitates the Cannizzaro reaction (conversion of DHA or glyceraldehyde to LAC) under oxidative conditions, likely facilitated by Lewis acidic or basic sites on the catalyst. The latter reduces or eliminates the need for base. However, the presence of oxygen can lead to formation of undesired side products, such as glyceric acid, tartronic acid, and glycolic acid – reducing chemoselectivity for lactic acid. A more atom-economical and selective alternative is the dehydrogenation of glycerol with liberation of H_2, albeit in the presence of base. A summary of the heterogeneous catalysts reported for glycerol dehydrogenation and conversion to lactic acid in the past decade is provided in Table 1.

2.2.1 Monometallic catalysts. Supported precious metal catalysts based on Pt, Au, Ir, Rh, Ru and Pd afford reasonable activity for the process, with varying degrees of selectivity. The lower selectivity relative to homogeneous catalysts stems from the co-formation of C1–C3 alcohols (1,2-propanediol (1,2-PDO), 1,3-propanediol (1,3-PDO), ethylene glycol (EG)), acids (glyceric and formic), as well as glycerol etherification products.

Group 10. In 2013 Chaudhari and Subramaniam[35] reported that the oxidant-free dehydrogenation of glycerol (and other biopolyols) in alkaline aqueous solution using various metal-based supported catalysts. Of these, Pt/C afforded highest chemoselectivity for LAC, 1,2-PDO and other C1–C3 alcohols at 160 °C, with 36.5%, 25.6% and 21.6% respectively, with a TON of 184 for LAC.[35] Vieira[36] found that selectivity and activity could be enhanced by reducing Pt particle size, achieving 65% and 74% selectivity respectively at 90 and 230 °C. Further reduction of particle size with hydrogen reduction of the catalyst at higher temperatures (500 °C) significantly enhanced Pt/C selectivity to 98%, with LAC yield of 93% and TOFs 3967 h^{-1} at 160 °C with KOH.[15] Notably, the authors also showed that a volcano-plot dependence between the initial rates of LAC formation by metal-loaded carbon catalysts and the difference between d–band center (ε_d) and Fermi energy (E_F) (Fig. 4). The highest initial rate was achieved by Pt/C, suggesting Pt has optimal interaction strength between the intermediates and the metal surface.

The Lewis acidic ZrO_2 was also explored as a support for highly dispersed Pt: Pinel *et al.* (2015)[37] reported that Pt on ZrO_2 is a more efficient catalyst for the reaction than Pt/TiO_2 and Pt/C under comparable conditions. The authors also showed that the system was applicable to crude glycerol, which afforded lower reaction rate but comparable selectivity to pure glycerol for LAC (~80%) at 180 °C.

Table 1 Activity of supported Group 10 catalysts for acceptorless dehydrogenation of glycerol and corresponding process metrics. All processes are in batch, with the exception of those with Time designation indicating "Flow"

Catalyst	LAC yield (%)	LAC Sel. (%)	Temp. (°C)	Time (h)	Max TOF (h^{-1})[b]	Energy economy coefficient (ε $°C^{-1}$ min^{-1})	*E* factor	ξ environmental energy impact factor	Base (base : gly mol ratio)	Ref.
Pt/C	29	36.5	160	6	179	5.03×10^{-6}	NA	NA	NaOH (1 : 1)	Chaudhari and Subramaniam (2013)[35]
Pt/C	73	74	230	3	119	1.76×10^{-5}	29.70	1.68×10^{6}	NaOH (1.1 : 1)	Vieira (2017)[36]
Pt/C	93	98	160	18	3967	5.38×10^{-6}	0.79	1.47×10^{5}	KOH (1.1 : 1)	Shimizu (2017)[15]
Pt/ZrO_2	80	84	180	8	[a]	9.26×10^{-6}	25.48	2.75×10^{6}	NaOH (1.8 : 1)	Pinel (2015)[37]
PtO_2/ZnO	68	80	240	Flow	2632	NA	NA	NA	NaOH (1 : 1)	Manfro (2018)[38]
Pd/C	68	71	230	3	1064	1.64×10^{-5}	31.93	1.94×10^{6}	NaOH (1 : 1)	Vieira (2015)[39] and Vieira (2017)[36]
Pd/HAP	94	95	230	1.5	1274	4.54×10^{-5}	5.35	1.18×10^{5}	NaOH (1 : 1)	Yin & Wang (2018)[40]
Ni^0/C	90	92	230	3	60	2.17×10^{-5}	11.77	5.41×10^{5}	NaOH (1.1 : 1)	Yin & Wang (2018)[41]
Ni^0/HAP	87	95	200	2	107	3.63×10^{-5}	5.87	1.62×10^{5}	NaOH (1.1 : 1)	Yin & Wang (2018)[42]
Ni-NiOx/C	47	49	200	0.5	18	7.83×10^{-5}	22.59	1.94×10^{6}	NaOH (1.1 : 1)	Liu & Li (2020)[43]

[a] Could not be calculated based on data provided. [b] TOFs in this review were extracted from the original articles or calculated from data provided therein.

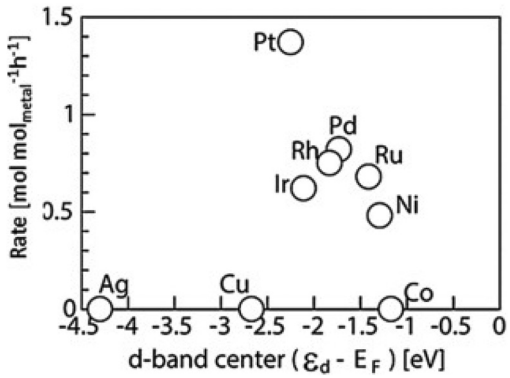

Fig. 4 Effect of difference between d-band center of the metals (ε_d) and Fermi energy (E_F) on the initial reaction rates for glycerol dehydrogenation by metal-loaded carbon catalysts. Reproduced from ref. 15 with permission from John Wiley and Sons, copyright 2017.

All the of the above catalysts were tested in batch, with limited discussion of catalyst stability. To fill that gap, Manfro *et al.*[51] explored the use of Lewis acidic supports for Pt, namely ZnO, MgO, Al_2O_3 in a continuous flow reaction system at 200–260 °C. Reaction conditions were adapted to reduce viscosity of glycerol solution (10 vol% glycerol solution) and reduce base concentration to minimize reactor clogging. Highest LAC selectivity and yield (80% and 68%) were obtained with Pt/ZnO at 240 °C with NaOH/glycerol molar ratio of 1, with 1,2-propanediol (1,2-PDO) as the second most abundant product. The catalysts showed excellent stability without evidence of deactivation over the evaluated period.

Vieira *et al.* concluded that Pd/C was less active and selective than Pt/C (10% Pd/C afforded 99% conversion with LAC selectivity of 68% at 230 °C with NaOH).[36] Shortly thereafter, Yin & Wang (2018)[40] showed that selectivity of supported Pd was significantly improved with a hydroxyapatite (HAP) support. Pd/HAP exhibits significantly higher LAC selectivity than Pd/C (95%, with 99% glycerol conversion) under the same conditions, resulting in 1274 turnovers per h. At different Pd loadings the catalysts possess different ratios of Pd^0 and Pd^{2+} species, with the catalyst with highest Pd^0 population affording highest activity (3% Pd/HAP). Interestingly, temperature-programmed desorption (TPD) studies showed that this was also the catalyst with highest density of strong basic sites, suggesting Pd loading modifies the acid–base properties of the catalytic system. The Pd_3/HAP catalyst could be recycled five times without a significant decrease in activity and LAC selectivity, but with minor Pd leaching. Generally, despite the inferior activity of Pd *vs.* Pt for this reaction (Fig. 4), supported Pd catalysts can be optimized to be selective for glycerol dehydrogenation, especially on basic supports. Although initial data suggests they are fairly robust,[39,40] most have not been tested under flow conditions to evaluate longevity.

As a much cheaper and more abundant group 10 metal, Ni has also been explored for this reaction. Based in the volcano plot of differences in d-band center and Fermi energy of metals and initial reaction rates (Fig. 4), nickel could be expected to have lower activity than Pt ad Pd, following the trend Pt > Pd > Ni, and this is indeed what is observed.[15] Yin & Wang found that Ni supported on HAP[42] and graphite (carbon)[41] were both active, albeit much less so than comparable Pd counterparts (*e.g.* TONs of Pd/C *vs.* Ni/C were 1064 *vs.* 60 h^{-1} under comparable conditions) (Table 1). More recently, Li *et al.* demonstrated that graphitic-carbon-layer-encapsulated Ni–NiO_x core/shell (Ni–NiO_x@C) catalyst (Ni–NiOx@C) afforded 49% yield of LAC in 30 min at temperatures below 200 °C, where the reaction synergistically promoted by base, metallic nickel and the acidic NiO_x acidic sites,[43] which accelerated the bond cleavage of α-C–H and C–O. However, the high nickel loading relative to other processes results in comparably lower TOF of 18 h^{-1}.

Group 11. The use of HAP as support spurred the design of a multifunctional, ternary nanohybrid catalysts consisting of

Table 2 Activity of supported Group 11 catalysts for acceptorless dehydrogenation of glycerol and corresponding process metrics. All processes are in batch, with the exception of those with Tiime designation indicating "Flow"

Catalyst	LAC yield (%)	LAC Sel. (%)	Temp. (°C)	Time (h)	Max TOF (h^{-1})	Energy economy coefficient (ε $°C^{-1}$ min^{-1})	*E* factor	ξ environmental energy impact factor	Base (base : gly mol ratio)	Ref.
CuO/Al_2O_3	77	79	240	6	1.2	8.91×10^{-6}	13.77	1.55×10^{6}	NaOH (1.1 : 1)	Chaudhari (2011)[44]
Cu_2O/CaO	50	54	190	1.25	3	3.51×10^{-5}	NA	NA	CaO (0.3 : 1)	Ye (2015)[45]
Cu/ZrO_2	95	95	180	8	2	1.10×10^{-5}	7.78	7.08×10^{5}	NaOH (1 : 1)	Liu & Dong (2016)[46]
Cu/HAP	90	90	230	2	116	3.26×10^{-5}	11.74	3.60×10^{5}	NaOH (1.1: 1)	Wang (2016)[47]
Cu^0 Nps	90	92	230	4	22	1.63×10^{-5}	11.77	7.22×10^{5}	NaOH (1.1: 1)	Yin (2017)[48]
Cu_2O Nps	75	87	230	2	8	2.72×10^{-5}	14.34	5.28×10^{5}	NaOH	Shen & Yin (2017)[49]
CuO	75	67.9	155	4	13	2.02×10^{-5}	2.50	1.24×10^{5}	NaOH (1.5 : 1)	Li (2020)[50]
CuO/MgO	~80	~90	240	flow	WHSV = 2 h^{-1}	NA	NA	NA	NaOH (1: 1)	ManFro (2016)[51]
Cu^0 /ZIF-8	84	89	230	6.5	NA.	9.36×10^{-6}	NA	NA	NaOH (1.5 : 1)	Xiao (2021)[52]
Cu-Cu_2O@NC -400	84.8	84.8	220	1.5	NA.	8.29×10^{-5}	55.20	6.66×10^{5}	-	Zhang & Chen (2022)[53]
CaO-supported CuO	58	93.6	230	4	2.9	3.52×10^{-5}	NA	NA	$Ca(OH)_2$ (0.8 : 1)	Yin (2022)[54]
CaO-supported Cu	96	97.1	230	4	4.8	4.28×10^{-5}	10.85	2.53×10^{5}	$Ca(OH)_2$ (0.8 : 1)	Yin (2022)[54]
Au/HAP/BN	99.5	99.5	100	2	[a]	1.05×10^{-5}	9.98	9.49×10^{5}	NaOH (1 : 1)	Bharath & Banat (2020)[55]
Au/Bentonite	76	92	90	4	[a]	1.74×10^{-5}	5.63	3.24×10^{5}	NaOH (8 : 1)	Yildiz (2020)[56]

[a] Could not be calculated based on data provided.

Au supported on two-dimensional boron nitride (BN) nanosheets and hexagonal hydroxyapatite (HAP) (Au/HAP/BN) (Table 2). The localized surface of BN was shown to exhibit high adsorption affinity for glycerol, while dual catalytic sites of Au and HAP catalyzed the dehydrogantion.[55] Full glycerol conversion and highly selective production of LAC (99.5%) were obtained at 100 °C in 2 hours. Reusability experiments showed the chemical stability of Au/HAP/BN, suggesting the catalyst is robust under reaction conditions. Monometallic Au catalysts are also studied with bentonite,[56] forming a catalyst that achieved LAC selectivity of 92.3%, but with 8-fold excess of NaOH to glycerol.

While the early investigation of copper on carbon supports suggested it is not active (Fig. 4),[15] we now know that this abundant group 11 metal shows significant promise as a catalyst for this reaction, albeit at higher temperatures relative to more precious metals. Cu nanoparticles (Nps) and Copper oxides have been studied on various of supports, as shown in Table 2. Chaudhari *et al.* showed that CuO/Al_2O_3 is an efficient catalyst for this reaction at 200–250 °C with excess aqueous base.[44] Although the TOFs were low (1.2 at 240 °C), the catalyst showed reasonable LAC selectivity (78.6%) and excellent recyclability. Liu & Dong showed that CuO on another acidic support, ZrO_2, was comparable in efficiency at 30% Cu loading (94.6% selectivity and quantitative conversion), albeit under slightly milder conditions, and provided highest selectivity for LAC among the Cu catalysts.[46]

To directly probe the effect of the acid–base properties of the support, Wang *et al.* examined Cu^0 on ZrO_2, MgO and HAP (hydroxyapatite), showing that basic supports (HAP and MgO) afford higher activity than the acidic, with Cu/HAP affording 116 turnovers per hour at 230 °C and 90% LAC selectivity.[47] However, the low glycerol concentration used (1 mol L^{-1}) would need to be increased to show industrial applicability. Manfro *et al.* tested the potential of supported Cu catalysts under flow conditions using a fixed bed reactor. Among Al_2O_3, ZnO and MgO as supports, Cu/MgO showed highest weight hourly space velocity (WHSV) of 2 h^{-1} at 240 °C.[51]

Ye *et al.* studied the potential synergistic effect of CaO as a solid base and Cu, CuO and Cu_2O as catalysts, finding glycerol conversion and LAC yield follow the trend Cu_2O > CuO > Cu.[45] The use of CaO reduces corrosion associated with the use of soluble hydroxide bases, such as NaOH or KOH, and allows the recycling of excess base *via* calcination, reverting $Ca(OH)_2$ back to CaO. When Cu_2O was immobilized on CaO, the glycerol conversion and LAC yield increased marginally compared to the physical mixture of CaO and Cu_2O.[45] The mechanism proposed involves glycerol deprotonation by CaO, Cu-catalyzed hydride abstraction to glyceraldehyde and dehydration to 2-hydroxypropenal. The latter converts to pyruvaldehyde *via* keto–enol tautomerization. Cu-catalyzed hydrogenation affords 1,2-PDO, while CaO-assisted intramolecular Cannizzaro reaction forms calcium lactate (Fig. 5).

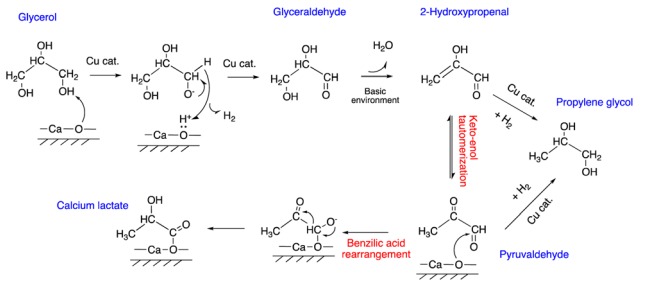

Fig. 5 Reaction pathway from glycerol to lactic acid and propylene glycerol with CaO and copper-based catalyst.[47]

While increasing the quantity of CaO relative to glycerol provides some gains in conversion and yield, it also decreases carbon balance, likely *via* base-assisted oligomerization resulting from glyceroxide ion and/or pyruvaldehyde. The higher molecular weight products can result in residues that get deposited on the solid catalysts, decreasing carbon balance or causing catalyst deactivation.

In a recent study by Yin *et al.*, CaO-supported metallic Cu catalysts demonstrated superior catalytic activity compared to CaO-supported CuO catalysts, the trend of which was different from the findings in Ye *et al.* The Cu(8)/CaO and Cu(16)/CaO catalysts, in particular, yielded glycerol conversions ranging from 91.4% to 98.8% and selectivities of lactic acid ranging from 91.1% to 97.1% when the glycerol dehydrogenation was performed at 230 °C for 4–6 hours using a catalyst/glycerol weight ratio of 5 : 100 and a $Ca(OH)_2$/glycerol molar ratio of 0.8 : 1.

Xiao *et al.* reported nano-Cu^0-supported zeolitic imidazolate framework (ZIF-8) catalyst for glycerol dehydrogenation to lactic acid.[52] The Cu/ZIF-8 is readily synthesized at room temperature with controllable morphology, and affords 84% yield (89% selectivity) of LAC in 6.5 h at 230 °C and 15% Cu loading. After four cycles, however, the yield drops to 68%, likely linked to the partial oxidation of Cu and irreversible adsorption of reaction components and by-products on the Cu/ZIF-8 surface. Most recently, Zhang and Chen *et al.* carried out the catalytic dehydrogenation of glycerol to lactic acid under N_2 atmosphere using highly dispersed Cu^0 and Cu_2O nanoparticles encapsulated by N-doped C (Cu-Cu_2O@NC), which were prepared by calcining Cu-based MOF.[53] The Cu-Cu_2O@NC-400 catalyst was found to have 100% glycerol conversion with 84.8% selectivity towards lactic acid at 220 °C for 90 minutes. Furthermore, the Cu-Cu_2O@NC-400 catalyst remained highly effective after being reused eight times with negligible loss of catalytic activity.

Unsupported Cu^0 NP, prepared by wet chemical reduction with mean size of 118 nm, afford only 22 h^{-1},[48] lower than that obtained with Cu^0 immobilized on basic supports, but comparable to the smaller polyethylene glycol (PEG)-modified Cu^0.[48] Unsupported Cu_2O NPs appear to be less active than the Cu0, with size-dependent activity (smaller nanoparticles showing higher activity).[49] In a systematic study by Li *et al.* to investigate the effect of anion and oxidation state of copper salts ($CuBr_2$, CuBr, $CuCl_2$, CuCl, CuF_2, $Cu(NO_3)_2$,CuO, and Cu_2O), the authors found that all salts were reduced to metallic copper with different morphologies during the reaction, and divalent CuO afforded highest yield. The latter was ascribed to their greater heat of reduction and highest local reaction temperature.[50]

In summary, we see evidence that supported Cu catalysts are potentially promising as cheap and reasonably selective catalysts for this process. Unfortunately, the disparate studies make it challenging to draw conclusions about the effect of support properties on activity and selectivity, as this depends on Cu phase; however, we do see examples of selective and active Cu catalysts on both acidic and basic supports.

Group 9. The success of Ir-based homogeneous catalysts for this reaction undoubtedly spurred the exploration of supported analogs of group 9 metals (Table 3). Modeled on the Ir N-heterocyclic carbene motif, Tu *et al.*[57] developed robust Ir-NHC co-polymers, which afford near-quantitative yield and selectivity of lactic acid at >3000 turnovers per hour at 115–165 °C. The catalyst was impressively stable, retaining activity and selectivity after 31 cycles. While no detectable leaching was observed, the coordination of iridium in the used catalyst was not probed. Oberhauser *et al.* intentionally formed Ir nanoparticles (*ca.* 1.8 nm) by decomposing an Ir(I) NHC complex under hydrogen reduction conditions.[58] Interestingly, while the resulting 'naked' NPs were highly active for glycerol dehydrogenation in 1,4-dioxane (TOF of 10^4 h^{-1}), analogous particles supported on carbon and tested in water were less active (~4000 h^{-1}), suggesting support effects and solvent dependence. Pinel *et al.*[59] examined Ir/C and Ir/$CaCO_3$, and noted a significant support effect: Ir/$CaCO_3$ was less active than Ir/C, even at 2-fold excess of NaOH to glycerol (Table 3). Pinel also examined an analogous Rh/C catalyst, which

Table 3 Activity of supported Group 9 catalysts for acceptorless dehydrogenation of glycerol and corresponding process metrics. All processes are in batch mode

Catalyst	LAC yield%	LAC sel.%	Temp. (°C)	Time (h)	Max TOF (h^{-1})	Energy economy coefficient (ε $°C^{-1}$ min^{-1})	*E* factor	ξ environmental energy impact factor	Base (base : glycerol mol ratio)	Ref.
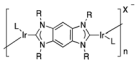	92	99	115–165	24	3444	5.56×10^{-6}	1.63	2.93×10^5	KOH (1 : 1)	Tu (2015)[57]
0.6% Ir/C	37	49	180	8	554	4.28×10^{-6}	55.88	1.30×10^7	NaOH (2 : 1)	Pinel (2011)[59]
Ir/$CaCO_3$	18	86	180	6	21	2.78×10^{-6}	117.96	4.25×10^7	NaOH (2 : 1)	Pinel (2011)[59]
Ir Nps	84	91	145	8	10 000	1.21×10^{-5}	3.16	2.62×10^5	NaOH (1 : 1)	Oberhauser (2018)[58]
Rh/C	25	45	180	8	399	2.89×10^{-6}	83.51	2.89×10^7	NaOH (2 : 1)	Pinel (2011)[59]
Rh/C	33	38	220	6	120	4.17×10^{-6}	32.47	7.79×10^6	NaOH (1.1 : 1)	Chaudhari and Subramaniam (2013)[35]
Co_3O_4/CeO_2	68	80	250	8	3	5.67×10^{-6}	1.20	2.12×10^5	NaOH (1.1 : 1)	Hernandez (2018)[60]
Co_3O_4/ZrO_2	67	73	250	8	NA	5.58×10^{-6}	NA	NA	NaOH (1 : 1)	López (2020)[61]

showed slightly lower activity and selectivity (TON of 399 *vs.* 504 h^{-1}).[59] Rh catalysts are less studied due to their lower activity and higher cost compared to the alternatives:[35,59] for example, Rh/C was also shown to be less active than Pt/C by Chaudhari and Subramaniam, with relative TOFs of 120 *vs.* 179 h^{-1}.[35]

While supported cobalt catalysts are significantly less active in comparison to later Group 9 metals, recent reports suggest that cobalt oxides on acidic supports could be effective under harsher conditions. For examples, in 2018, Hernandez *et al.*[60] reported that Co_3O_4/CeO_2 affords 68% LAC yield and 80% selectivity under 250 °C in 8 h. Comparable results were achieved with Co_3O_4/ZrO_2 affording 67% LAC yield with 73% selectivity.[61]

2.2.2 Bimetallic/trimetallic systems. Bimetallic and trimetallic systems have also been studied and shown to be efficient for the conversion of glycerol to lactic acid. In particular, several examples of bimetallic/trimetallic catalysts that include Cu combined with Pd,[62] Au,[63] Ru[64] and base metals, such as Zn/Al[64] show promising activity for dehydrogenation, as shown in Table 4. Wang & Yin (2017)[65] showed unsupported bimetallic $CuAu_x$ nanoparticles exhibited higher catalytic activity for the conversion of concentrated glycerol (2–3 M) to lactic acid than either monometallic Cu and Au nanoparticles, implicating synergy in the alloyed nanoparticles. However, the system is still not particularly active based on TOF per the formula unit, achieving only ~8 turnovers per h (Table 4). Activation energies for glycerol conversion are positively correlated with ratio of Cu, namely 64.0, 53.4, 46.8, and 36.9 kJ mol^{-1} for $CuAu_1$, $CuAu_2$, $CuAu_3$, and $CuAu_4$ respectively. Comparable TOFs were obtained with unsupported $CuPd_x$ nanoparticles by Yin & Wang (2019),[62] who also noted synergistic effects between the two metals for this reaction. Under optimal conditions (2 mol% catalyst at 220 °C for 2 h), selectivity for lactic acid using $CuPd_2$, $CuPd_3$, and $CuPd_4$ was >90% and comparable for the three catalysts,[62] suggesting lower sensitivity of reaction rate to Cu : Pd ratio than that in the case of unsupported $CuAu_x$ NPs.

Upon supporting $CuAu_{0.8}$ particles on a ceria support the activity appears to increase significantly (TOF per formula unit) – to 258 turnovers per hour at 220 °C, and stable for up to 4 cycles.[63] However, since the experiments for unsupported and supported are reported at different temperatures, it is not possible to make a definitive conclusion.

In the case of Pt–Co/CeO_x there appears to be a significant synergy between the two metals suggested by the higher activity observed for the bimetallic *vs.* monometallic species (Table 4,[66]). The latter is attributed to strong electronic coupling between Pt and Co, which likely forms a dual-site that can activate both glycerol and base.[66] The ceria support is suggested to provide electron-donation, which suppresses side reactions from C–C and C–O bond cleavage.

A trimetallic catalyst, Ru–Zn–Cu(I) immobilized on hydroxyapatite (HAP) has also been reported, affording lactic acid in 71% yield. The authors suggest that introducing Cu^+ significantly improves selectivity for lactic acid by inhibiting undesired C–C bond cleavage.[64] The catalyst could be reused at least four times without significant activity loss.

2.2.3 Base-free systems. Given that the use of homogeneous bases (*i.e.*, NaOH) significantly increases *E*-factors, especially if lactic acid, rather than the lactate salt, is the desired product, we examined the alternatives. While base-free conditions are possible in some heterogeneous systems cited below, they all involve oxidative processes. For example, Liu *et al.* (2013) reported AuPd/TiO_2 with Lewis acidic $AlCl_3$;[67] Heeres reported Au–Pt catalysts on zeolites supports;[68] Fan *et al.* (2014) reported Pt-Sn/MFI(zeolites)[69] and Hara *et al.*[32] reported Pt-PVP (polyvinylpyrrolidone) on TiO_2 Shishido (2020)[31] described a bifunctional catalyst containing Pt nanoparticles (NPs) and layered-Nb_2O_5(L-Nb_2O_5). The challenge with oxidative processes is overoxidation products. Despite this, selectivity up to 81% for lactic acid have been obtained.[69] Thus, a comparison in terms of process efficiency between a more selective dehydrogenative process and a base-free but less selective oxidative one would depend on the efficiency of the separation of lactic acid from the latter reaction medium. Thus, while oxidative processes have selectivity challenges compared to dehydrogenative ones, they should not be discounted, especially if they can be coupled with efficient lactic acid separation processes.

Table 4 Activity of bi/tri-metallic heterogeneous catalysts for acceptorless dehydrogenation of glycerol and corresponding process metrics

Bi/tri-metallic	LAC yield (%)	LAC Sel. (%)	Temp. (°C)	Time (h)	Max TOF (h^{-1})	Energy economy coefficient (ε $°C^{-1}$ min^{-1})	*E* factor	ξ environmental energy impact factor	Base (base : glycerol mol ratio)	Ref.
Group 11										
$CuAu_x$	93	94	200	2	8[a]	3.88×10^{-5}	5.41	1.40×10^{5}	NaOH (1.1 : 1)	Wang & Yin (2017)[65]
Cu-Zn-Al	95	96	175	4	NA	2.26×10^{-5}	2.97	1.31×10^{5}	NaOH (1.1 : 1)	Li (2017)[71]
$Au_{0.8}Cu/CeO_2$	71	91	220	8	258[b]	6.72×10^{-6}	26.00	3.87×10^{6}	NaOH (1 : 1)	Palacio (2019)[63]
Group 11–10										
$CuPd_2$ Nps	90	91	220	2	8[c]	3.41×10^{-5}	5.59	1.64×10^{5}	NaOH (1.1 : 1)	Yin & Wang (2019)[62]
Group 10–9										
$Pt_{0.7}$-$Co_{0.2}$/CeOx	75	88	200	4	1534[d]	1.56×10^{-5}	48.77	3.12×10^{6}	NaOH (1 : 1)	Jin & Yang (2019)[66]
Group 11–8										
Ru-Zn-Cu(I)/HAP	83	83	140	21	3[e]	4.14×10^{-6}	27.52	6.65×10^{6}	NaOH (1.5 : 1)	Han (2017)[64]

[a] TOF is calculated based on mol of $CuAu_2$. [b] Based on Au. [c] Based on mol of $CuPd_2$. [d] Based on Pt. [e] Based on Ru.

2.3 Green Chemistry metrics of catalysts towards glycerol dehydrogenation

Akbulut and Özkar noted that none of the papers they reviewed on glycerol dehydrogenation reported green chemistry metrics.[70] Given that environmental impact for these catalytic processes should be reported, here we apply three green chemistry metrics that facilitate comparison for homogeneous *vs.* heterogeneous methods. The metrics, namely environmental energy impact (ξ), energy economy factor (ε), and *E* factor, are calculated for each or the reports reviewed and shown in Tables 1–5.

The calculated process metrics enable us to compare the environmental impact of various studies in order to determine their relative feasibility and connect viable implementations for these catalytic processes. However, *E*-factor calculations assume heterogeneous catalysts are effectively recycled, which is not always the case.

Table 5 summarizes the most active heterogeneous catalysts from each metal Group, as well as the most active homogeneous catalysts. Optimal process would have low *E*-factor and environmental energy impact (ξ), but a high energy economy factor (ε). Fig. 6 depicts the results by plotting the environmental energy impact (ξ) and energy economy factor (ε) values. Based on these trends, Group 11 (entries 1–4, Table 5) and one Group 10 report (entry 7, Table 5) have favorable process metrics, namely low Environmental energy impact (ξ) and high energy economy factor (ε). Compared to the heterogeneous processes, the most robust homogeneous processes (entries 15–18, Table 5) are less favorable in terms of both factors considered. It is also prudent to highlight that these metrics do not capture the holistic impact of the processes, with the biggest drawback that they do not account for the lack of recovery of precious metals from the homogenous processes. While the lack of recovery does not result in less favorable *E*-factors, the use of precious metals should be captured by new metrics that capture the waste associated with their mining and manufacturing.

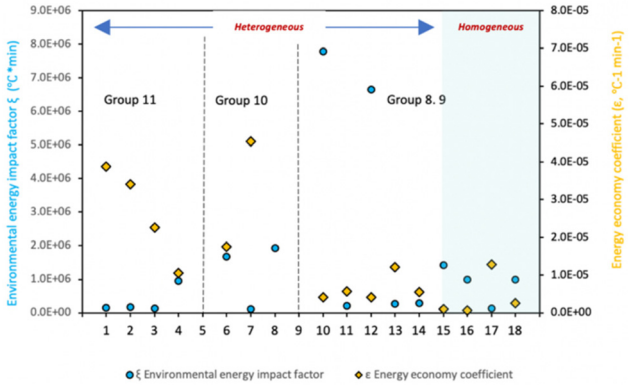

Fig. 6 Environmental energy impact (ξ), energy economy factor (ε) for the most select reports of glycerol dehydrogenation to lactic acid, including both heterogeneous and homogeneous catalysts.

We also assessed the Environmental, Health and Safety (EHS), Clean Chemistry, and Greenness scores[144] for the additive (NaOH or KOH). The latter scores are described in the preceeding reference. NaOH and KOH have identical scores of 7, 9, 8, which indicated low concern.

3. Acceptorless dehydrogenation of ethanol

The rapid growth of the global bioethanol market over the last two decades, fueled by burgeoning interest in new cellulosic biomass processing methods, has eventually pushed annual

Table 5 Summaries of the green process metrics for the most active homogeneous and heterogeneous catalysts for glycerol dehydrogenation to lactic acid, all reported in batch

Entry	Catalyst	Energy economy coefficient (ε °C^{-1} min^{-1})	*E* factor	ξ environmental energy impact factor (°C min^{-})	Ref.
	Group 11				
1	$CuAu_x$	3.88×10^{-5}	5.41	1.40×10^{5}	Wang & Yin (2017)[65]
2	$CuPd_2$ Nps	3.41×10^{-5}	5.59	1.64×10^{5}	Yin & Wang (2019)[62]
3	Cu–Zn–Al	2.26×10^{-5}	2.97	1.31×10^{5}	Li (2017)[71]
4	Au/HAp/BN	1.05×10^{-5}	9.98	9.49×10^{5}	Bharath & Banat (2020)[55]
	Group 10				
6	Pt/C	1.76×10^{-5}	29.70	1.68×10^{6}	Vieira (2017)[36]
7	Pd/HAP	4.54×10^{-5}	5.35	1.18×10^{5}	Yin & Wang (2018)[40]
8	Ni–NiOx/C	7.83×10^{-5}	22.59	1.94×10^{6}	Liu & Li (2020)[43]
	Group 8, 9				
10	Rh/C	4.17×10^{-6}	32.47	7.79×10^{6}	Chaudhari and Subramaniam (2013)[35]
11	Co_3O_4/CeO_2	5.67×10^{-6}	1.20	2.12×10^{5}	Hernandez (2018)[60]
12	Ru–Zn–Cu(I)/HAP	4.14×10^{-6}	27.52	6.65×10^{6}	Han (2017)[64]
13	NHC-stab. Ir Nps	1.21×10^{-5}	3.16	2.62×10^{5}	Oberhauser (2018)[58]
14	Ir polymer	5.56×10^{-6}	1.63	2.93×10^{5}	Tu (2015)[57]
15	Homo. Ir cat. **1**	1.06×10^{-6}	1.52	1.43×10^{6}	Crabtree (2014)[16]
16	Homo. Ir cat. **2**	6.16×10^{-7}	0.61	9.86×10^{5}	Williams (2016)[17]
17	Homo. Ir cat. **3**	1.28×10^{-5}	1.65	1.29×10^{5}	Voutchkova-Kostal (2018)[18]
18	Homo. Ir cat. **4**	2.59×10^{-6}	2.55	9.85×10^{5}	Jang (2020)[19]

global ethanol production above 100 billion liters.[72] This increase in output has sparked intense research into the use of bioethanol reforming to produce hydrogen and other valuable chemicals. The most basic pathway is ethanol dehydrogenation to acetaldehyde, which results in the release of one equivalent of hydrogen gas. This reaction is of high interest, as acetaldehyde is an important reactive intermediate in organic syntheses and can be a versatile platform for the formation of ethyl acetate,[73] acetic acid,[74] acetic anhydride,[75] and butyl aldehyde[76] (Scheme 4). Additionally, acetaldehyde can undergo further reactions to yield coupled products, such as 1-butanol[77] and 1,3-butadiene.[78,79] The traditional production of acetaldehyde *via* the Wacker process involves the direct catalytic oxidation of ethylene, generating chlorinated waste.[80] Thus, dehydrogenation of bioethanol is significantly more atom-economical, justifying research into the discovery and improvement of catalysts for this process.

3.1 Homogeneous catalysts

In the last decade, there has been a rapid growth in reports for ethanol dehydrogenation using both homogeneous and heterogeneous catalysts. Among homogeneous catalysts, group 8 compounds have been the most extensively studied catalysts for this process. Milstein *et al.* showed that while PNP–Ru(II) catalyst can facilitate dehydrogenation of ethanol at low temperatures (−30 °C), the resulting aldehydes were trapped by the catalyst as an aldehyde adduct with the Ru and PNP pincer ligand (Scheme 5).[81]

A density functional theory study by Yang[82] suggested that the nature of the N-ligand is critical for facilitating the dehydrogenation of ethanol. Specifically, an analog of aliphatic PNP pincer ruthenium complex **6** (Fig. 7), (PNP)Ru(H)CO, where PNP = bis[2-(diisopropylphosphino)ethyl]amino, proceeds *via* a N-assisted deprotonation of ethanol and ethanol-assisted transfer of a proton from ligand nitrogen to the metal

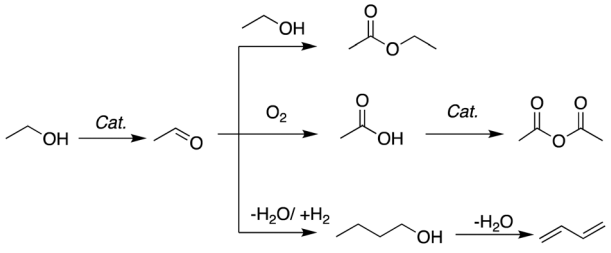

Scheme 4 Products from initial dehydrogenation of ethanol.

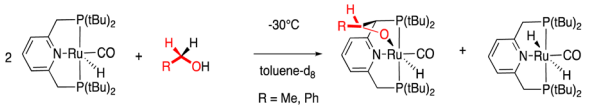

Scheme 5 Dehydrogenation of ethanol by a PNP–Ru(II) at −30 °C, but resulting in aldehydes adducts. Reproduced from ref. 81 with permission from American Chemical Society, copyright 2012.

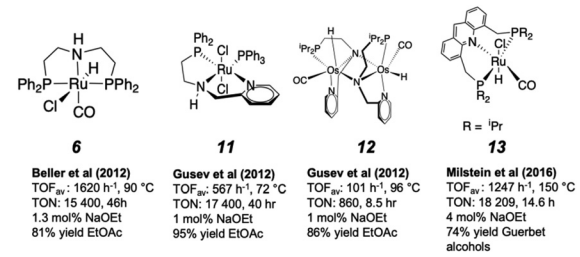

Fig. 7 Ruthenium and Osmium homogeneous catalysts for ethanol dehydrogenation.

center for the formation of H_2 (Scheme 6). This elucidated the differences in catalytic activity between the aromatic and aliphatic pincer ligands in ruthenium complexes. The study also suggested that an iron PNP pincer analog may have lower energy barrier of ethanol dehydrogenation than the Ru analog.[82]

Considering insight from theory, Beller *et al.* showed that aliphatic Ru-PNP, also known as Takasago catalyst or Ru-MACHO, (**6**, Fig. 7) affords TOF 1134 h^{-1} in refluxing ethanol (~1600 h^{-1} at 90 °C and 50 ppm Ru), while the Ir analog showed negligible activity.[83] Their study confirmed that aliphatic PNP pincer ligands on a ruthenium-based system are critical to achieving activity in this reaction. However, the reaction produced only ethyl acetate *via* dehydrogenative coupling (Scheme 7), and no acetaldehyde. In fact, aldehyde inhibited

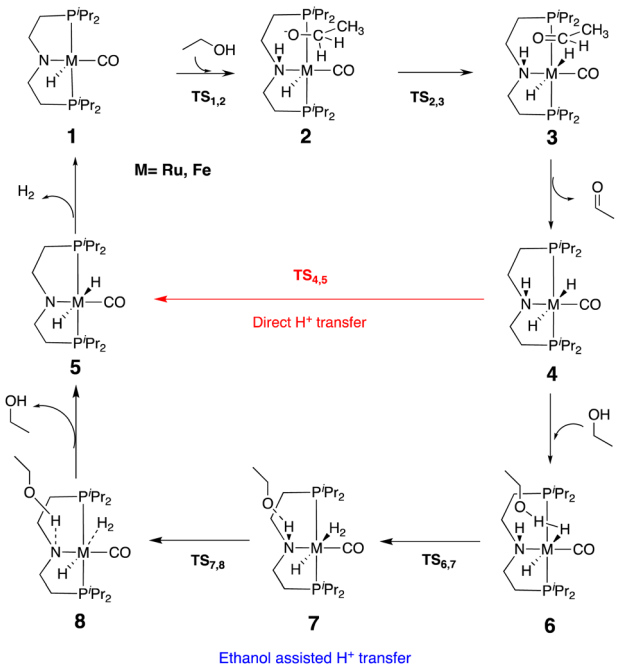

Scheme 6 Catalytic cycle for the dehydrogenation of ethanol by aliphatic (PNP)Ru(H)CO, proposed by Yang,[82] showing direct proton transfer (Red) and ethanol-bridged proton transfer pathways for the formation of H2 and acetaldehyde. Reproduced from ref. 82 with permission from American Chemical Society, copyright 2013.

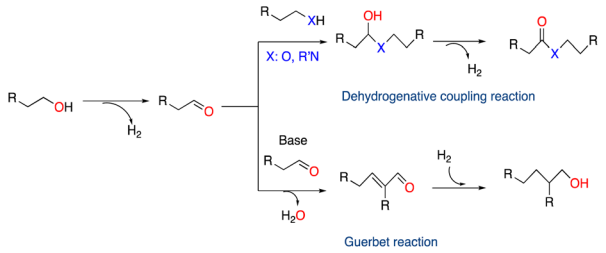

Scheme 7 Ethanol dehydrogenation as initial step to dehydrogenative coupling or Guerbet process.

the catalyst, suggesting that the concentration of "free" aldehyde should be minimized during the reaction. Gusev *et al.*[84] shortly thereafter showed that replacing a phosphine with a hemilabile pyridine affords a similarly active, air-stable catalyst – Ru-NNP complex **11**, which achieved 567 h^{-1} at ethanol reflux temperatures. Under catalytic conditions, both **6** and **11** produce the Ru(II) amido species by HX elimination, which are subsequently protonated by ROH to afford alkoxide intermediates that undergo β-hydrogen elimination and H_2 loss, and regenerate the catalyst. Later, Gusev *et al.* also showed that the more abundant osmium dimer (**12**) affords significant activity for the reaction in the absence of base (101 h^{-1}), exceeding the activity of the Ru dimer analog.[85]

Considering insight from theory, Beller *et al.* showed that aliphatic Ru-PNP, also known as Takasago catalyst or Ru-MACHO, (**6**, Fig. 7) affords TOF 1134 h^{-1} in refluxing ethanol (~1600 h^{-1} at 90 °C and 50 ppm Ru), while the Ir analog showed negligible activity.[83] Their study confirmed that aliphatic PNP pincer ligands on a ruthenium-based system are critical to achieving activity in this reaction. However, the reaction produced only ethyl acetate *via* dehydrogenative coupling (Scheme 7), and no acetaldehyde. In fact, aldehyde inhibited the catalyst, suggesting that the concentration of "free" aldehyde should be minimized during the reaction. Gusev *et al.*[84] shortly thereafter showed that replacing a phosphine with a hemilabile pyridine affords a similarly active, air-stable catalyst – Ru-NNP complex **11**, which achieved 567 h^{-1} at ethanol reflux temperatures. Under catalytic conditions, both **6** and **11** produce the Ru(II) amido species by HX elimination, which are subsequently protonated by ROH to afford alkoxide intermediates that undergo β-hydrogen elimination and H_2 loss, and regenerate the catalyst. Later, Gusev *et al.* also showed that the more abundant osmium dimer (**12**) affords significant activity for the reaction in the absence of base (101 h^{-1}), exceeding the activity of the Ru dimer analog.[85]

In 2016 Milstein *et al.* reported that acridine-based Ru-PNP analog (**13**), which achieved high ethanol conversion (73%) at 150 °C, but *via* an alternative Guerbet process, forming a mix of butanol, hexanol and octanol with a maximum TOF of 1247 h^{-1} (Scheme 7).[86] The yield and selectivity depend on the base used, which is consistent with the need for base to catalyze the aldol condensation step of the process. DFT studies suggest ethanol coordinates *cis* to the Ru–H, which allows the ethanol hydroxyl to protonate the Ru–H and liberate H_2. The latter is followed by β-H elimination of the Ru-ethoxide to complete the cycle. Since the product of the aldol condensation undergoes double hydrogenation to form the Guerbet alcohol, the process can also be considered a net transfer hydrogenation from ethanol to the aldol condensate (Scheme 7).

3.2 Heterogeneous catalysts

Considering the scale of the ethanol dehydrogenation process, it is evident that cost-effective and resilient heterogeneous catalysts would possess a distinct edge over their homogeneous counterparts. The trends observed between ethanol dehydrogenation to acetaldehyde and metal, particle size, morphology, and support are highlighted in the following discussion. Readers seeking a more exhaustive examination of heterogeneous catalysts utilized in ethanol dehydrogenation throughout the last twenty years are encouraged to consult a recent review authored by Yang and Cui.[87]

3.2.1 Cu-based catalysts. To date, the majority of ethanol dehydrogenation to acetaldehyde has been studied over Cu-based heterogeneous catalysts due to their high selectivity for the dehydrogenation of various alcohol feedstocks.[88] For instance, in a study comparing Cu, Ni, Co and Ce catalysts on activated carbon (AC) supports, Jongsomjit *et al.* showed that ethanol dehydrogenation to acetaldehyde was strongly favored over the Cu/AC catalysts between 250 and 400 °C, while the Co and Ce-based catalysts performed only on par with the unmodified activated carbon support[89] (Table 6). Ni/AC facilitated primarily dehydration rather than dehydrogenation at temperatures above 350 °C.

The use of metal oxides, such as SiO_2,[90–95] Al_2O_3,[96] ZnO[97,98] and MgO[99] as supports for Cu-based dehydrogenation catalysts has been widely studied. Such supports possess relatively high surface area and often facilitate strong metal–support interactions. Recent work has demonstrated that the design of multi-component support materials, like mixed metal oxides, can be advantageous to tuning the electronic properties of the support, and thus catalyst activity. For example, Busca *et al.* demonstrated the activity of Cu on spinel supports such as $ZnAl_2O_4$ and $MgAl_2O_4$, achieving >90% acetaldehyde yield; however, increases in reaction temperature or time gradually shifted selectivity towards other dehydration products, such as diethyl ether and ethylene.[109] Hou *et al.* reported a highly dispersed Cu catalyst, $Cu_{1.4}/Zn_{3.2}Mg_{1.4}Al_2O_{7.6}$, at a temperature of 280 °C, a pressure of 0.1 MPa, and a WHSV of 11.8 h^{-1}, the catalyst displayed outstanding activity in the dehydrogenation of ethanol to acetaldehyde, with acetaldehyde and H_2 selectivity exceeding 98.5%.[119] Cu supported on a high surface area zeolite was investigated by Li *et al.*, where the zeolite support stabilized Cu active sites, affording acetaldehyde yields of ~70% (~90% acetaldehyde selectivity, TOF = 24 h^{-1}) for over 100 hours.[100] Steady deactivation occurred after 100 hours *via* Cu reduction and sintering, with the decrease in catalyst activity only partially recovered after catalyst regeneration. One limiting factor in using metal oxides as supports for Cu-based

Table 6 Heterogeneous ethanol dehydrogenation catalysts and corresponding selectivity for acetaldehyde. Most processes are in continuous flow, with the exception of those with a numerical indicator of reaction Time (h), indicating batch mode. In those cases reaction time is equivalent to residence time

	Acetaldehyde							
Catalyst	Yield (%)	Sel. (%)	Conversion (%)	Time (h)	TOF (h^{-1})	Temp. (°C)	TOF/Temp. (h^{-1} °C^{-1})	Ref.
Cu								
Cu-MFI(silica)	90	93	97	Flow	4	250	0.016	Zhang (2020)[95]
Cu/MFI	93	95.7	97.2	Flow	10	250	0.040	Zheng (2023)[94]
Cu/zeolite	77	90	85	Flow	24	300	0.080	Dai (2019)[100]
Cu (zeolite encapsulated)	80	90	88	Flow	—	250	NA.	Luo (2022)[101]
Cu-ZnO/MCM-41	19	93	20	Flow	756	225	3.360	Gallo (2020)[102]
Cu-HT	74	99	75	Flow	234	300	0.780	Silva (2018)[103]
Cu-HT	80	99	81	Flow	15	250	0.060	Perez-Lopez (2018)[104]
Cu/SiO_2 metal foam	37	97	38	Flow	0.9	275	0.003	Chladek (2008)[105]
Cu/Ca_2O_4Si	38	95	40	Flow	64	270	0.237	Okamoto (2018)[106]
CuNi/SiO_2	25	100	25	Flow	9	250	0.036	Flytzani-Stephanopoulos (2017)[107]
Cu/Al_2O_3	80	90	89	Flow	119	200	0.595	Cassinelli & Santilli (2015)[108]
Cu/$ZnAl_2O_4$	88	96	92	Flow	—	300	NA.	Busca (2020)[109]
Cu-Ni/$MgAlO_x$	39	99	40	Flow	324	260	1.246	Galvita & Thybaut (2020)[110]
Cu–Ca–Al	91	98	93	1	13	250	0.052	Perez-Lopez (2019)[111]
Cu/ZrO_2, TiO_2, Al–ZrO_2	—	100	—	—	288	210	1.371	Christopher (2019)[112]
Cu/$Cu_2Cr_2O_5$	54	90	60	Flow	0.9	200	0.005	Santacesaria (2012)[113]
Cu/mesoporous C	79	95	83	Flow	27	280	0.096	Lu (2015)[114]
Cu/AC	63	96	65	Flow	267	350	0.763	Jongsomjit (2019)[89]
Cu/PPC (polyacrylonitrile-based porous carbon)	76	95	80	Flow	27	260	0.104	Lu (2017)[115]
Cu/N-doped graphite	19–29	>95	20–30	Flow	31	250	0.124	Guerrero-Ruiz (2016)[116]
Cu/C/SiO_2	79	95	83	Flow	32	260	0.123	Lu (2018)[117]
Cu/SiO_2/SiC	76	94	81	Flow	54	280	0.193	Lu (2019)[118]
CuNP /mesoporous SiO_2	96.8	100	96.8	Flow	NA	250	NA.	Yang (2022)[93]
Cu-SiO_2 (prepared by aerosol-assisted sol–gel)	55	100	55	Flow	NA	300	NA.	Garbarino & Debecker (2023)[92]
$Cu_{1.4}/Zn_{3.2}Mg_{1.4}Al_2O_{7.6}$	NA	98.5	NA	Flow	NA	280	NA.	Hou (2022)[119]
Precious metals								
Pd/ZnO	14	100	14	Flow	43	155	0.277	Ouyang (2020)[120]
Ag/CeO_2	90	95	95	Flow	13	325	0.040	Mamontov (2016)[121]
Au/$Zn_1Zr_{10}Ox$	75	94	80	Flow	422	325	1.298	Flytzani-Stephanopoulos (2015)[122]
PdZn/HT	NA	98	NA	Flow	NA	260	NA	Galvita & Thybaut (2017)[123]
Multimetal (precious)								
Au/$MgCuCr_2O_4$	95	95	100	Flow	807	250	3.228	Liu & Hensen (2013)[124]
Au/Cu/SiO_2	94	80–90	90	Flow	220	200	1.100	Dai (2012)[125]
Cu, Ag, Cu–Ag/C	NA	10	NA	Flow	13–355	250	NA	Morales (2019)[126]
Others								
Mg–Al	30	65	46	Flow	NA	350	NA	Jongsomjit (2019)[127]
MCF-C (mesocellular carbon foam)	14	80	17	Flow	0.18	400	0.0005	Jongsomjit (2020)[128]
Zn/SiO_2 (Silicalite-1)	61.6	94.5	65.2	Flow	NA	400	NA	Kegnæs (2022)[129]
(Zr + Ce)O_2–Al_2O_3	17.7	75.8	23.4	NA	NA	380	NA	Chuklina & Zhukova (2022)[130]

ethanol dehydrogenation is that the surface acidity/basicity can lead to C–O bond cleavage and ethanol dehydration to ethylene or coupling to C3+ compounds (*via* condensation or ketonization).[109] Luo *et al.* reported a ultra-small Cu nanoclusters (~1.8 nm) encapsulated in Silicate-1, which performs on par with the Cu/zeolite with less sintering due to the spatial constraint environment effectively limits the mobility of Cu entities during catalysis. Additionally, this environment promotes a substantial quantity of well-maintained Cu^+ species (up to approximately 70%), which are crucial in improving the catalyst's overall performance.[101]

Carbon-based supports have been widely implemented for ethanol dehydrogenation over Cu catalysts,[128,131,132] as they exist in many forms, and their physiochemical properties can be tuned. For instance, a high surface area mesoporous carbon (MC) support was compared to mesoporous silica (SBA-15) by Lu *et al.*[133] The Cu-MC achieved superior TOF (27.5 h^{-1} *vs.* 25.7 h^{-1}) and acetaldehyde selectivity (95% *vs.* 82%), which was attributed to the inert MC preventing side reactions typically promoted by surface –OH and/or –COOH on the SBA-15. These results were reinforced in a follow-up study, which compared Cu catalysts supported on carbon, SiO_2 and carbon-coated SiO_2.[117] The lowest ethanol TOF (14 h^{-1}) was observed over the Cu/C catalyst, which underwent deactivation within 10 h on stream. Higher ethanol TOFs were observed for both Cu/C/SiO_2 (32 h^{-1}) and Cu/SiO_2 (33 h^{-1}) but the selectivity towards acetaldehyde over Cu/C/SiO_2 (95%) was superior to Cu/SiO_2 (79%) due to the suppression of secondary side reactions *via* the formation of an inert carbon layer in the C/SiO_2 support.

The inert surface of carbon supports offers both thermal and chemical stability. However, it also gives rise to only weak interactions with metal surfaces. These weak metal–carbon interactions may render metals that readily sinter, such as Cu, to easily agglomerate on the support surface and rapidly deactivate at elevated reaction temperatures.[91,134–136] As such, functionalization of the carbon support has been investigated in numerous recent studies, with an eye to enhancing metal–support interactions while maintaining stability and surface area. For instance, in comparing graphene materials as Cu supports, Guerrero-Ruiz *et al.* demonstrated that Cu supported on nitrogen-functionalized graphene oxide yields small Cu particles with strong metal–support interactions.[116] These strong interactions gave rise to high catalytic stability at 250 °C, while the hydrophobicity of the support reduced side reactions arising from the presence of water. In a similar study of a porous carbon support N-doped with polyacrylonitrile, a highly dispersed Cu phase was obtained, which was resistant to agglomeration.[115]

In conclusion, the extant literature concerning Cu catalysts utilized in ethanol dehydrogenation indicates that the characteristics of the support material exert a significant impact on both acetaldehyde selectivity and catalyst deactivation. In pursuit of this objective, catalyst support selection seems to involve two principal strategies: (i) the utilization of inert supports composed of carbon materials serves to diminish the likelihood of side reactions taking place at specific active sites within the support material; and (ii) the implementation of metal oxide supports featuring robust metal–support interactions hinders Cu deactivation *via* sintering. A recurring theme in the literature suggests that the optimization of TOF might be achievable through the modification or engineering of support structures, irrespective of whether carbon or metal oxide supports are employed. To stabilize small, sinter-resistant Cu NPs with a high relative surface area, the support should be modifiable to provide the strong metal–support interactions required, but should not contain active sites that promote undesirable side reactions. Although modifications to carbon-based supports have been effective in restricting Cu sintering, mixed metal oxides are superior as supports for Cu catalysts, as shown in Table 6's selectivity, temperatures, and TOFs.

3.2.2 Non-Cu containing catalysts. In attempts to overcome the stability and selectivity issues of Cu-based ethanol dehydrogenation catalysts, Cu-free catalysts have been explored. In 2016 Flytzani-Stephanopoulos *et al.* reported the use of atomically dispersed Au catalysts on a mixed $ZnZrO_x$ support.[122] The atomic dispersion of Au gives rise to Au–O_x–ZnO active sites, which have proven dehydrogenation activity.[137] Brønsted acid sites on the ZrO_2 surface were minimized *via* a combination adding basic ZnO and passivation by Au cations, which was suggested to lead to high TOF ($422h^{-1}$) and quantitative selectivity for acetaldehyde and hydrogen at temperatures below 300 °C. These results suggest Au-based catalysts could be promising candidates for the dehydrogenation of ethanol to acetaldehyde and further oxidation of acetaldehyde to acetic acid by mobile surface oxygen species. However, it is important to note that metallic Au nanoparticles are plagued by the same deactivation *via* sintering and agglomeration as Cu, which limits their longevity at moderate-to-high reaction temperatures.[138]

Ag supported on mixed CeO_2/SiO_2[121] has also been explored for this reaction by Mamontov *et al.*, achieving moderate TOF ($13\ h^{-1}$) of a dilute stream of ethanol with near quantitative selectivity for acetaldehyde at 400 °C. The CeO_2 doping of the silica support provided a synergistic activity between the acidic $Ag^{\delta+}$ sites and the basic CeO_2 surface. Unfortunately, the stability of these catalysts was not probed, as Ag is known to deactivate at elevated temperatures.[139]

Particle size and site isolation have a critical role in controlling selectivity[120] and stability in Pd/ZnO catalysts for this reaction. Low Pd loading on ZnO synthesized *via* solvothermal method afforded single-atom dispersion of Pd in defect sites, affording 100% selectivity for acetaldehyde and resistance to coke formation, potentially masking competing ethanol dehydration and decomposition. The maximum acetaldehyde yield was ~20% (TOF $43\ h^{-1}$) at the reaction temperature of 165 °C. In contrast, Pd clusters supported on commercial ZnO showed undesirably high selectivity (20%) towards CO and CH_4 formation *via* C–C scission, rather than ethanol dehydrogenation *via* C–H bond scission.

Recent explorations of metal-free catalytic ethanol dehydrogenation have been implemented with some success. Jongsomjit *et al.* studied calcined Mg–Al layered double hydroxides, demonstrating that a metallic phase is not necessary to achieve ethanol conversion.[127] The low conversion of ethanol (18% at 400 °C) could be increased (up to 65%) by introducing O_2 to the reaction, but this resulted in rapid oxidation of acetaldehyde to CO_2 on the metal oxide surface and thereby decreased acetaldehyde selectivity drastically. In another study from the Jongsomjit group, a high surface area mesocellular carbon foam exhibited high acetaldehyde selectivity[128] (80–100%), albeit at moderate ethanol conversion (17%). Interestingly, even in the absence of an active metal phase, moderate catalyst deactivation occurred over the carbon foam due to collapse of the porous structure and subsequent loss of surface area. While metal-free catalysts offer a new perspective for ethanol dehydrogenation, the yields of acetaldehyde achieved so far remain well below what is possible for even the most rudimentary supported Cu catalysts.

Chuklina & Zhukova reported zirconia-alumina mixed oxides $(Zr + Ce)O_2 + Al_2O_3$ to be active for ethanol dehydrogenation, where the selectivity towards acetaldehyde was highly dependent on the oxide composition.[130] At a low ZrO_2/Al_2O_3 ratio, these catalysts promoted the formation of diethyl ether through Lewis acid sites primarily composed of an aluminum–oxygen environment, which facilitated the interaction between an ethoxy group and an activated nondissociated ethanol molecule.

Most recently, Kegnæs *et al.* revealed that MFI zeolites containing Zn were also effective catalysts with high activity and selectivity for the given process.[129] Specifically, the optimal

catalyst consists of Silicalite-1 zeolite with 5 wt% Zn, resulting in 65.2% conversion and 94.5% selectivity towards acetaldehyde when operated at 400 °C. The author attributed the high selectivity to the absence of Brønsted acidic sites (*i.e.*, Incorporating Zn reduced the presence of acidic silanol groups that may promote the formation of dehydration products).

3.2.3 Bimetallic catalysts. Rather than replacing Cu as the active metal, many recent studies have examined the addition of a second metal species as a method of enhancing catalyst performance. Flytzani-Stephanopoulos *et al.* found that addition of Ni to a Cu supported on SiO_2 significantly increased catalyst reactivity by lowering the barrier to C–H bond activation, thereby increasing ethanol conversion without altering the high selectivity towards acetaldehyde.[140] However, addition of Pt and Pd did not improve Cu catalyst performance, suggesting they acted as spectators in the reaction. This potentially contradicts the findings of Sykes *et al.*, who found that adding 1 wt% Pt to a Cu surface yielded a six-fold increase in ethanol dehydrogenation,[141] but the disparity could be explained by the lack of a support material. The primary role of the Pt sites was to enhance O–H bond activation, but Flytzani-Stephanopoulos *et al.* showed that this is often achieved by the support material, leaving the C–H bond activation as the rate-limiting step. Microkinetic modeling over metal surfaces carried out by Haider *et al.* supported the above suggestion that C–H bond activation limits the performance of Cu-based catalysts.[142] Furthermore, the modeling results showed that alloying Cu with Ni, Pd, Pt or Rh increases the theoretical TOF of ethanol, which seems to support the findings of both Flytzani-Stephanopoulos *et al.* and Sykes *et al.* Alloying Cu with Ag decreases ethanol dehydrogenation, according to Guerrero-Ruiz *et al.*, as the addition of Ag blocks active Cu sites with far less active Ag sites.[126] This is partially backed by the modeling of Haider *et al.*, where Ag was not only less likely to activate ethanol, but also had a high selectivity towards dehydration to ethylene.[142]

3.3 Summary and outlook

The reported ethanol dehydrogenation processes suggest that catalytic activity is highly dependent on the active catalyst and support. While several studies have shown that homogeneous Ru-PNP catalysts have promising activity for the AD of ethanol, they rarely typically produce C4/C6/C8 alcohols instead of just acetaldehyde *via* a Guerbet process. Even if those are the desired products, the existing homogeneous processes are still a challenge to scale due to the large amounts of rare earth metals required.

Ethanol dehydrogenation has been studied more extensively over heterogeneous catalysts, with copper-based being prominent in the literature. Mixed metal oxide supports that offer robust support interactions and characteristic surface acidity/basicity tend to exhibit superior performance in comparison to inert carbon supports, as demonstrated by Cu-based systems, based on ethanol TOF and catalyst lifetime. Under milder conditions, supported precious metal catalysts (Pd, Ag, or Au) provide higher ethanol TOF in comparison to Cu. However, this strategy does not alleviate catalyst deactivation. The effect of combining Cu with precious metals may be promising on both counts, but is not yet systematically elucidated. For example, Flytzani-Stephanopoulos *et al.* suggest that Pd and Pt act as spectators,[140] while Sykes *et al.* observed a six-fold increase in TOF over a Pt–Cu surface.[141]

The process performance metrics used to assess the dehydration of glycerol were not suitable for ethanol dehydrogenation. The product distribution varies drastically, as does the desired product, making the use of green chemistry process metrics challenging. This is because while lactic acid is the desired product in almost all cases above, for ethanol dehydrogenation there may be distinct desired products. Furthermore, most ethanol dehydrogenation reactions were carried out in a continuous mode, rather than the batch processes used for glycerol, making contact time between reactant and catalyst is difficult to assess. Residence time and space velocity would also serve as useful metrics for catalyst comparison, but data for calculation of the latter were only available for a few of the entries, given that most reports were fundamental studies of catalyst efficiency, catalyst structure–activity relationships, mechanistic studies, and catalyst stability. Separation studies were seldom reported in these reports, and so metrics that include the material and energy efficiency of separations could not be provided. However, we sought to provide an alternative metric to capture catalyst efficiency and that can be calculated based on available data. We thus report the ratio of catalyst turnover frequency as a ratio of reaction temperature for the flow studies. Higher value suggests higher catalyst efficiency with lower energy input.

The recent shift in catalyst prescreening *via* computational methods has been explored for alcohol dehydrogenation by Michel *et al.*[143] Ethanol dehydrogenation to formaldehyde and hydrogen was studied over Co, Ni, Pt, Rh, Ir, Pd, Os, Ru and Re surfaces using first principles (DFT) and micro-kinetic calculations, which revealed that the reaction is most thermodynamically favored over Pt surfaces. Furthermore, when expanding the analysis to consider 294 dilute alloys, 12 candidates with high catalyst potential were identified. While this work considered neither Cu catalysts nor dehydrogenation of ethanol, it serves as a fine example of utilizing theoretical analyses and paves the way for future studies. Ultimately, such methods are integral in designing new heterogeneous catalysts that approach the performance of their homogeneous counterparts.

4. Conclusions

Catalytic processes have the potential to foster a circular economy through the utilization of waste materials and the development of novel chemical compounds that enable reversible processes. The former facilitates the conversion of waste low-value streams into valuable materials and provides more immediate means of closing the loop on existing processes to enable circularity; the latter provides significantly more potent

tools for innovating new chemistry and gaining a competitive edge.[18]

Glycerol and ethanol, derived from renewable sources, are particularly promising substrates for valorization. While conversion processes of these substrates can vary considerably, the vast majority commence with alcohol dehydrogenation (AD).

While many homogeneous and heterogeneous processes have been reported for glycerol AD and conversion to lactic acid, almost none report or compare to existing processes based on green chemistry metrics.[70] Given that environmental impact for these catalytic processes should be reported, here we apply three green chemistry metrics that facilitate comparison for homogeneous *vs.* heterogeneous methods. The metrics, namely environmental energy impact (ξ), energy economy factor (ε), and *E* factor, are calculated for each or the reports reviewed.

AD of glycerol to lactic acid was first demonstrated by homogeneous catalysts in the presence of stoichiometric base. The most active catalysts are based on iridium NHC complexes, which readily outperform heterogeneous catalysts based on TOF. However, a significant drawback of homogeneous catalysts is their challenging recovery from the reaction, rendering them non-reusable. While the lack of recovery does not result in less favorable *E*-factors, the use of precious metals should be captured by new metrics that capture the waste associated with their mining and manufacturing.

Supported catalysts containing precious metals, such as Pt, Au, Ir, Rh, Ru, and Pd, demonstrate considerable activity for glycerol dehydrogenation, albeit with varying degrees of selectivity. The reduced selectivity compared to homogeneous catalysts arises from the simultaneous formation of C1–C3 alcohols, acids, and glycerol etherification products. Based on analysis of green process metrics, most of Group 11 and some of Group 10 heterogeneous catalysts have most favorable process metrics, namely low Environmental energy impact (ξ) and high energy economy factor (ε).

To better facilitate the catalytic dehydrogenation of glycerol to LAC, the following aspects need to be further addressed: (i) reducing the dependence on precious metals by either transitioning to more readily available metals or developing robust, heterogeneous catalysts. (ii) Ensuring excellent stability and recyclability of catalysts to enable their repeated usage in multiple cycles. (iii) Overcoming mass transfer limitations caused by the high base concentration and elevated viscosity of the medium. (iv) Implementing strategies for neutralizing acid salts (such as lactate) and separating lactic acid from the reaction mixture.

Switching gears to the second substrate considered herein, ethanol, we report the dominance of heterogenous catalysts for the acceptorless dehydrogenation of this substrate. Here, the choice of active catalyst has a significant impact on the catalytic activity and lifetime. Among heterogeneous catalysts for this process, copper-based catalysts have been shown most promising, where support materials have drastic impact on activity. Mixed metal oxide supports outperform inert carbon based on selectivity, TOF and catalyst stability. This is due to the strong metal–support interactions and tunable surface acidity/basicity of the latter. Substituting the active Cu metal with precious metals, including Pd, Ag, or Au, usually increases TOF and allows for use of lower reaction temperature. However, this approach does not necessarily resolve catalyst deactivation issues, and adds urgency to ensure full catalyst recovery so as to reduce waste of precious metal.

Ru-PNP catalysts have shown the most promise among the homogeneous catalysts studied for the process. However, most Ru-based homogeneous catalysts do not produce acetaldehyde and instead undergo dehydrogenative coupling to form ethyl acetate or the Guerbet process to produce C4+ alcohols. This selectivity problem is compounded by the need to develop viable homogeneous alternatives that do not rely on large quantities of rare earth metals.

Author contributions

The manuscript was written through contributions of all authors. All authors have given approval to the final version of the manuscript.

Conflicts of interest

There are no conflicts to declare.

Acknowledgements

We thank NSF Chemistry (award # 2154815 and # 1805080) for financial support.

References

1 U. EPA, Typical Wastes Generated by Industry Sectors https://www.epa.gov/hwgenerators/typical-wastes-generated-industry-sectors#q5.
2 J. Paterson, M. Peacock, R. Purves, R. Partington, K. Sullivan, G. Sunley and J. Wilson, *ChemCatChem*, 2018, **10**, 5154–5163.
3 T. Schubert, *Biofuels Bioprod. Biorefin.*, 2020, **14**, 845–878.
4 C. Gunanathan and D. Milstein, *Science*, 2013, **341**, 1229712.
5 R. H. Crabtree, *Chem. Rev.*, 2017, **117**, 9228–9246.
6 B. Subramaniam, P. Licence, A. Moores and D. T. Allen, *ACS Sustainable Chem. Eng.*, 2021, **9**, 3977–3978.
7 E. Barnard, J. J. R. Arias and W. Thielemans, *Green Chem.*, 2021, **23**, 3765–3789.
8 H. W. Tan, A. R. Abdul Aziz and M. K. Aroua, *Renewable Sustainable Energy Rev.*, 2013, **27**, 118–127.
9 J. ten Dam and U. Hanefeld, *ChemSusChem*, 2011, **4**, 1017–1034.

10 A. Villa, G. M. Veith and L. Prati, *Angew. Chem. Int. Ed.*, 2010, **49**, 4499–4502.
11 V. R. Ruiz, A. Velty, L. L. Santos, A. Leyva-Pérez, M. J. Sabater, S. Iborra and A. Corma, *J. Catal.*, 2010, **271**, 351–357.
12 M. H. Haider, N. F. Dummer, D. Zhang, P. Miedziak, T. E. Davies, S. H. Taylor, D. J. Willock, D. W. Knight, D. Chadwick and G. J. Hutchings, *J. Catal.*, 2012, **286**, 206–213.
13 M. Dusselier, P. Van Wouwe, A. Dewaele, E. Makshina and B. F. Sels, *Energy Environ. Sci.*, 2013, **6**, 1415–1442.
14 S. Lux, P. Stehring and M. Siebenhofer, *Sep. Sci. Technol.*, 2010, **45**, 1921–1927.
15 S. M. A. H. Siddiki, A. S. Touchy, K. Kon, T. Toyao and K. i. Shimizu, *ChemCatChem*, 2017, **9**, 2816–2821.
16 L. S. Sharninghausen, J. Campos, M. G. Manas and R. H. Crabtree, *Nat. Commun.*, 2014, **5**, 5084.
17 Z. Lu, I. Demianets, R. Hamze, N. J. Terrile and T. J. Williams, *ACS Catal.*, 2016, **6**, 2014–2017.
18 M. Finn, J. A. Ridenour, J. Heltzel, C. Cahill and A. Voutchkova-Kostal, *Organometallics*, 2018, **37**, 1400–1409.
19 Y. J. Cheong, K. Sung, J. A. Kim, Y. K. Kim and H. Y. Jang, *Eur. J. Inorg. Chem.*, 2020, **2020**, 4064–4068.
20 M. V. Jimenez, A. I. Ojeda-Amador, R. Puerta-Oteo, J. Martinez-Sal, V. Passarelli and J. J. Perez-Torrente, *Molecules*, 2022, **27**, 21.
21 Y. Li, M. Nielsen, B. Li, P. H. Dixneuf, H. Junge and M. Beller, *Green Chem.*, 2015, **17**, 193–198.
22 M. Dutta, K. Das, S. J. Prathapa, H. K. Srivastava and A. Kumar, *Chem. Commun.*, 2020, **56**, 9886–9889.
23 L. S. Sharninghausen, B. Q. Mercado, R. H. Crabtree and N. Hazari, *Chem. Commun.*, 2015, **51**, 16201–16204.
24 C.-Q. Deng, J. Deng and Y. Fu, *Green Chem.*, 2022, **24**, 8477–8483.
25 P. Lakshmanan, P. P. Upare, N.-T. Le, Y. K. Hwang, D. W. Hwang, U. H. Lee, H. R. Kim and J.-S. Chang, *Appl. Catal. A*, 2013, **468**, 260–268.
26 R. K. P. Purushothaman, J. v. Haveren, D. S. v. Es, I. Melián-Cabrera, J. D. Meeldijk and H. J. Heeres, *Appl. Catal. B*, 2014, **147**, 92–100.
27 Y. H. Shen, S. H. Zhang, H. J. Li, Y. Ren and H. C. Liu, *Chem. – Eur. J.*, 2010, **16**, 7368–7371.
28 C. Zhang, T. Wang and Y. Ding, *Catal. Lett.*, 2017, **147**, 1197–1203.
29 C. Zhang, T. Wang, X. Liu and Y. Ding, *Chin. J. Catal.*, 2016, **37**, 502–509.
30 C. Zhang, T. Wang and Y. J. Ding, *Catal. Lett.*, 2017, **147**, 1197–1203.
31 S. Feng, K. Takahashi, H. Miura and T. Shishido, *Fuel Process. Technol.*, 2020, **197**, 106202.
32 T. Komanoya, A. Suzuki, K. Nakajima, M. Kitano, K. Kamata and M. Hara, *ChemCatChem*, 2016, **8**, 1094–1099.
33 T. Komanoya, A. Suzuki, K. Nakajima, M. Kitano, K. Kamata and M. Hara, *ChemCatChem*, 2016, **8**, 1094–1099.
34 M. Tao, D. Zhang, H. Guan, G. Huang and X. Wang, *Sci. Rep.*, 2016, **6**, 29840.
35 X. Jin, D. Roy, P. S. Thapa, B. Subramaniam and R. V. Chaudhari, *ACS Sustainable Chem. Eng.*, 2013, **1**, 1453–1462.
36 M. R. A. Arcanjo, I. J. Silva, E. Rodríguez-Castellón, A. Infantes-Molina and R. S. Vieira, *Catal. Today*, 2017, **279**, 317–326.
37 J. Ftouni, N. Villandier, F. Auneau, M. Besson, L. Djakovitch and C. Pinel, *Catal. Today*, 2015, **257**, 267–273.
38 A. M. Bruno, C. A. Chagas, M. M. V. M. Souza and R. L. Manfro, *Renewable Energy*, 2018, **118**, 160–171.
39 F. L. Marques, A. C. Oliveira, J. M. Filho, E. Rodríguez-Castellón, C. L. Cavalcante and R. S. Vieira, *Fuel Process. Technol.*, 2015, **138**, 228–235.
40 L. Shen, Z. Yu, D. Zhang, H. Yin, C. Wang and A. Wang, *J. Chem. Technol. Biotechnol.*, 2019, **94**, 204–215.
41 H. Yin, H. Yin, A. Wang and L. Shen, *J. Ind. Eng. Chem.*, 2018, **57**, 226–235.
42 L. Qiu, H. Yin, H. Yin and A. Wang, *J. Nanosci. Nanotechnol.*, 2018, **18**, 4734–4745.
43 Z. Xiu, H. Wang, C. Cai, C. Li, L. Yan, C. Wang, W. Li, H. Xin, C. Zhu, Q. Zhang, Q. Liu and L. Ma, *Ind. Eng. Chem. Res.*, 2020, **59**, 9912–9925.
44 D. Roy, B. Subramaniam and R. V. Chaudhari, *ACS Catal.*, 2011, **1**, 548–551.
45 L. Liu and X. P. Ye, *Fuel Process. Technol.*, 2015, **137**, 55–65.
46 G.-Y. Yang, Y.-H. Ke, H.-F. Ren, C.-L. Liu, R.-Z. Yang and W.-S. Dong, *Chem. Eng. J.*, 2016, **283**, 759–767.
47 H. Yin, C. Zhang, H. Yin, D. Gao, L. Shen and A. Wang, *Chem. Eng. J.*, 2016, **288**, 332–343.
48 H. Yin, H. Yin, A. Wang, L. Shen, Y. Liu and Y. Zheng, *J. Nanosci. Nanotechnol.*, 2017, **17**, 1255–1266.
49 L. Shen, H. Yin, H. Yin, S. Liu and A. Wang, *J. Nanosci. Nanotechnol.*, 2017, **17**, 780–787.
50 K. T. Li and H. H. Li, *Appl. Biochem. Biotechnol.*, 2020, **191**, 125–134.
51 A. B. F. Moreira, A. M. Bruno, M. M. V. M. Souza and R. L. Manfro, *Fuel Process. Technol.*, 2016, **144**, 170–180.
52 K. Qiu, Y. Shu, J. Zhang, L. Gao and G. Xiao, *Catal. Lett.*, 2022, **152**, 172–186.
53 J. Zhang, X. Wu, J. Chen, X. Wang and Y. Mai, *ChemCatChem*, 2023, **15**, e202201139.
54 A. Wang, Q. Xu and H. Yin, *React. Kinet. Mech. Catal.*, 2022, **135**, 3205–3221.
55 G. Bharath, K. Rambabu, A. Hai, H. Taher and F. Banat, *ACS Sustainable Chem. Eng.*, 2020, **8**, 7278–7289.
56 B. Sever and M. Yildiz, *React. Kinet. Mech. Catal.*, 2020, **130**, 863–874.
57 Z. Sun, Y. Liu, J. Chen, C. Huang and T. Tu, *ACS Catal.*, 2015, **5**, 6573–6578.
58 W. Oberhauser, C. Evangelisti, A. Liscio, A. Kovtun, Y. Cao and F. Vizza, *J. Catal.*, 2018, **368**, 298–305.
59 F. Auneau, S. Noël, G. Aubert, M. Besson, L. Djakovitch and C. Pinel, *Catal. Commun.*, 2011, **16**, 144–149.

60 R. Palacio, S. Torres, D. Lopez and D. Hernandez, *Catal. Today*, 2018, **302**, 196–202.
61 S. Torres, R. Palacio and D. López, *Appl. Catal. A*, 2021, **621**, 118199.
62 L. Shen, X. Zhou, C. Zhang, H. Yin, A. Wang and C. Wang, *J. Food Biochem.*, 2019, **43**(8), 12931.
63 R. Palacio, D. López and D. Hernández, *J. Nanopart. Res.*, 2019, **21**, 148.
64 Z. Jiang, Z. Zhang, T. Wu, P. Zhang, J. Song, C. Xie and B. Han, *Chem. – Asian J.*, 2017, **12**, 1598–1604.
65 L. Shen, X. Zhou, A. Wang, H. Yin, H. Yin and W. Cui, *RSC Adv.*, 2017, **7**, 30725–30739.
66 G. Zhang, X. Jin, Y. Guan, B. Yin, X. Chen, Y. Liu, X. Feng, H. Shan and C. Yang, *Ind. Eng. Chem. Res.*, 2019, **58**, 14548–14558.
67 J. Xu, H. Zhang, Y. Zhao, B. Yu, S. Chen, Y. Li, L. Hao and Z. Liu, *Green Chem.*, 2013, **15**, 1520–1525.
68 R. K. P. Purushothaman, J. v. Haveren, A. Mayoral, I. Melián-Cabrera and H. J. Heeres, *Top. Catal.*, 2014, **57**, 1445–1453.
69 H. J. Cho, C.-C. Chang and W. Fan, *Green Chem.*, 2014, **16**, 3428–3433.
70 D. Akbulut and S. Özkar, *RSC Adv.*, 2022, **12**, 18864–18883.
71 K.-T. Li, J.-Y. Li and H.-H. Li, *J. Taiwan Inst. Chem. Eng.*, 2017, **79**, 74–79.
72 U. D. o. Energy, Global Ethanol Production by Country or Region, **https://afdc.energy.gov/data/10331/**(accessed March 2022).
73 A. G. Sato, D. P. Volanti, I. C. de Freitas, E. Longo and J. M. C. Bueno, *Catal. Commun.*, 2012, **26**, 122–126.
74 B. Venugopal, R. Kumar and N. R. Kuloor, *Ind. Eng. Chem. Process Des. Dev.*, 1967, **6**, 139–146.
75 B. H. Carpenter, *Ind. Eng. Chem. Process Des. Dev.*, 1965, **4**, 105–111.
76 H. A. Wittcoff, *J. Chem. Educ.*, 1983, **60**, 1044.
77 J. Zhang, K. Shi, Z. An, Y. Zhu, X. Shu, H. Song, X. Xiang and J. He, *Ind. Eng. Chem. Res.*, 2020, **59**, 3342–3350.
78 G. M. Cabello González, R. Murciano, A. L. Villanueva Perales, A. Martínez, F. Vidal-Barrero and M. Campoy, *Appl. Catal. A*, 2019, **570**, 96–106.
79 V. L. Sushkevich, I. I. Ivanova, V. V. Ordomsky and E. Taarning, *ChemSusChem*, 2014, **7**, 2527–2536.
80 M. Eckert, G. Fleischmann, R. Jira, H. M. Bolt and K. Golka, *Ullmann's Encyclopedia of Industrial Chemistry*, 2000.
81 M. Montag, J. Zhang and D. Milstein, *J. Am. Chem. Soc.*, 2012, **134**, 10325–10328.
82 X. Z. Yang, *ACS Catal.*, 2013, **3**, 2684–2688.
83 M. Nielsen, H. Junge, A. Kammer and M. Beller, *Angew. Chem. Int. Ed.*, 2012, **51**, 5711–5713.
84 D. Spasyuk and D. G. Gusev, *Organometallics*, 2012, **31**, 5239–5242.
85 D. Spasyuk, S. Smith and D. G. Gusev, *Angew. Chem. Int. Ed.*, 2012, **51**, 2772–2775.
86 Y. Xie, Y. Ben-David, L. J. W. Shimon and D. Milstein, *J. Am. Chem. Soc.*, 2016, **138**, 9077–9080.
87 Y. Huang, B. Wang, H. Yuan, Y. Sun, D. Yang, X. Cui and F. Shi, *Catal. Sci. Technol.*, 2021, **11**, 1652–1664.
88 R. M. Rioux and M. A. Vannice, *J. Catal.*, 2003, **216**, 362–376.
89 J. Ob-eye, P. Praserthdam and B. Jongsomjit, *Catalysts*, 2019, **9**(1), 66–79.
90 E. D. Guerreiro, O. F. Gorriz, J. B. Rivarola and L. A. Arrúa, *Appl. Catal. A*, 1997, **165**, 259–271.
91 A. J. Marchi, J. L. G. Fierro, J. Santamaría and A. Monzón, *Appl. Catal. A*, 1996, **142**, 375–386.
92 G. Pampararo, G. Garbarino, P. Riani, V. Vykoukal, G. Busca and D. P. Debecker, *Chem. Eng. J.*, 2023, **465**, 142715.
93 Y. Hao, D. Zhao, W. Liu, M. Zhang, Y. Lou, Z. Wang, Q. Tang and J. Yang, *Catalysts*, 2022, **12**, 1049.
94 J. Pang, M. Yin, P. Wu, L. Song, X. Li, T. Zhang and M. Zheng, *ACS Sustainable Chem. Eng.*, 2023, **11**, 3297–3305.
95 J. Pang, M. Zheng, C. Wang, X. Yang, H. Liu, X. Liu, J. Sun, Y. Wang and T. Zhang, *ACS Catal.*, 2020, **10**, 13624–13629.
96 G. Krishna Reddy, K. S. Rama Rao and P. Kanta Rao, *Catal. Lett.*, 1999, **59**, 157–160.
97 S.-i. Fujita, N. Iwasa, H. Tani, W. Nomura, M. Arai and N. Takezawa, *React. Kinet. Catal. Lett.*, 2001, **73**, 367–372.
98 H. Liu, Z. Chang, J. Fu and Z. Hou, *Appl. Catal. B*, 2023, **324**, 122194.
99 R. K. Marella, C. K. Prasad Neeli, S. R. Rao Kamaraju and D. R. Burri, *Catal. Sci. Technol.*, 2012, **2**, 1833–1838.
100 D. Yu, W. Dai, G. Wu, N. Guan and L. Li, *Chin. J. Catal.*, 2019, **40**, 1375–1384.
101 L. Lin, P. Cao, J. Pang, Z. Wang, Q. Jiang, Y. Su, R. Chen, Z. Wu, M. Zheng and W. Luo, *J. Catal.*, 2022, **413**, 565–574.
102 P. H. Finger, T. A. Osmari, M. S. Costa, J. M. C. Bueno and J. M. R. Gallo, *Appl. Catal. A*, 2020, **589**, 117236.
103 I. S. P. Campisano, C. B. Rodella, Z. S. B. Sousa, C. A. Henriques and V. Teixeira da Silva, *Catal. Today*, 2018, **306**, 111–120.
104 M. Rosset and O. W. Perez-Lopez, *React. Kinet. Mech. Catal.*, 2018, **123**, 689–705.
105 P. Chladek, E. Croiset, W. Epling and R. R. Hudgins, *Can. J. Chem. Eng.*, 2007, **85**, 917–924.
106 A. Segawa, A. Nakashima, R. Nojima, N. Yoshida and M. Okamoto, *Ind. Eng. Chem. Res.*, 2018, **57**, 11852–11857.
107 J. Shan, N. Janvelyan, H. Li, J. Liu, T. M. Egle, J. Ye, M. M. Biener, J. Biener, C. M. Friend and M. Flytzani-Stephanopoulos, *Appl. Catal. B*, 2017, **205**, 541–550.
108 W. H. Cassinelli, L. Martins, A. R. Passos, S. H. Pulcinelli, A. Rochet, V. Briois and C. V. Santilli, *ChemCatChem*, 2015, **7**, 1668–1677.
109 G. Pampararo, G. Garbarino, P. Riani, M. Villa García, V. Sánchez Escribano and G. Busca, *Appl. Catal. A*, 2020, **602**, 117710.

110 J. De Waele, V. V. Galvita, H. Poelman, M. Gabrovska, D. Nikolova, S. Damyanova and J. W. Thybaut, *Appl. Catal. A*, 2020, **591**, 117401.
111 M. Rosset and O. W. Perez-Lopez, *React. Kinet. Mech. Catal.*, 2018, **123**, 689–705.
112 S. Hanukovich, A. Dang and P. Christopher, *ACS Catal.*, 2019, **9**, 3537–3550.
113 E. Santacesaria, G. Carotenuto, R. Tesser and M. Di Serio, *Chem. Eng. J.*, 2012, **179**, 209–220.
114 Q.-N. Wang, L. Shi and A.-H. Lu, *ChemCatChem*, 2015, **7**, 2721–2721.
115 P. Zhang, Q.-N. Wang, X. Yang, D. Wang, W.-C. Li, Y. Zheng, M. Chen and A.-H. Lu, *ChemCatChem*, 2017, **9**, 505–510.
116 M. V. Morales, E. Asedegbega-Nieto, B. Bachiller-Baeza and A. Guerrero-Ruiz, *Carbon*, 2016, **102**, 426–436.
117 Q.-N. Wang, L. Shi, W. Li, W.-C. Li, R. Si, F. Schüth and A.-H. Lu, *Catal. Sci. Technol.*, 2018, **8**, 472–479.
118 M.-Y. Li, W.-D. Lu, L. He, F. Schüth and A.-H. Lu, *ChemCatChem*, 2019, **11**, 481–487.
119 H. Liu, Y. Jiang, R. Zhou, Z. Chang and Z. Hou, *Fuel*, 2022, **321**, 123980.
120 M. Ouyang, S. Cao, S. Yang, M. Li and M. Flytzani-Stephanopoulos, *Ind. Eng. Chem. Res.*, 2020, **59**, 2648–2656.
121 G. V. Mamontov, M. V. Grabchenko, V. I. Sobolev, V. I. Zaikovskii and O. V. Vodyankina, *Appl. Catal. A*, 2016, **528**, 161–167.
122 C. Wang, G. Garbarino, L. F. Allard, F. Wilson, G. Busca and M. Flytzani-Stephanopoulos, *ACS Catal.*, 2016, **6**, 210–218.
123 J. De Waele, V. V. Galvita, H. Poelman, C. Detavernier and J. W. Thybaut, *Catal. Sci. Technol.*, 2017, **7**, 3715–3727.
124 P. Liu and E. J. M. Hensen, *J. Am. Chem. Soc.*, 2013, **135**, 14032–14035.
125 J. C. Bauer, G. M. Veith, L. F. Allard, Y. Oyola, S. H. Overbury and S. Dai, *ACS Catal.*, 2012, **2**, 2537–2546.
126 J. M. Conesa, M. V. Morales, C. López-Olmos, I. Rodríguez-Ramos and A. Guerrero-Ruiz, *Appl. Catal. A*, 2019, **576**, 54–64.
127 P. Pinthong, P. Praserthdam and B. Jongsomjit, *J. Oleo Sci.*, 2019, **68**, 95–102.
128 Y. Klinthongchai, S. Prichanont, P. Praserthdam and B. Jongsomjit, *J. Environ. Chem. Eng.*, 2020, **8**, 103752.
129 K. Gao, J. Mielby and S. Kegnæs, *Catal. Today*, 2022, **405–406**, 144–151.
130 S. Chuklina, A. Zhukova, Y. Fionov, M. Kadyko, A. Fionov, D. Zhukov, A. Il'icheva, L. Podzorova and I. Mikhalenko, *ChemistrySelect*, 2022, **7**, e202203031.
131 F. Carrasco-Marín, A. Mueden and C. Moreno-Castilla, *J. Phys. Chem. B*, 1998, **102**, 9239–9244.
132 J. Ob-eye, P. Praserthdam and B. Jongsomjit, *Catalysts*, 2019, **9**(1), 66–79.
133 Q.-N. Wang, L. Shi and A.-H. Lu, *ChemCatChem*, 2015, **7**, 2846–2852.
134 J. T. Sun, I. S. Metcalfe and M. Sahibzada, *Ind. Eng. Chem. Res.*, 1999, **38**, 3868–3872.
135 A. Prašnikar, A. Pavlišič, F. Ruiz-Zepeda, J. Kovač and B. Likozar, *Ind. Eng. Chem. Res.*, 2019, **58**, 13021–13029.
136 S. Qing, X. Hou, L. Li, G. Feng, X. Wang, Z. Gao and W. Fan, *Int. J. Hydrogen Energy*, 2019, **44**, 16667–16674.
137 M. B. Boucher, N. Yi, F. Gittleson, B. Zugic, H. Saltsburg and M. Flytzani-Stephanopoulos, *J. Phys. Chem. C*, 2011, **115**, 1261–1268.
138 F. Yang, M. S. Chen and D. W. Goodman, *J. Phys. Chem. C*, 2009, **113**, 254–260.
139 V. A. Lavrenko, A. I. Malyshevskaya, L. I. Kuznetsova, V. F. Litvinenko and V. N. Pavlikov, *Powder Metall. Met. Ceram.*, 2006, **45**, 476–480.
140 J. Shan, J. Liu, M. Li, S. Lustig, S. Lee and M. Flytzani-Stephanopoulos, *Appl. Catal. B*, 2018, **226**, 534–543.
141 Z.-T. Wang, R. A. Hoyt, M. El-Soda, R. J. Madix, E. Kaxiras and E. C. H. Sykes, *Top. Catal.*, 2018, **61**, 328–335.
142 T. S. Khan, F. Jalid and M. A. Haider, *Top. Catal.*, 2018, **61**, 1820–1831.
143 T. Wang, J. Sha, M. Sabbe, P. Sautet, M. Pera-Titus and C. Michel, *Nat. Commun.*, 2021, **12**, 5100.
144 J. P. Adams, C. M. Alder, I. Andrews, A. M. Bullion, M. Campbell-Crawford, M. G. Darcy, J. D. Hayler, R. K. Henderson, C. A. Oare, I. Pendrak, A. M. Redman, L. E. Shuster, H. F. Sneddon and M. D. Walker, *Green Chem.*, 2013, **15**, 1542–1549.
145 B. M. Trost, *Angew. Chem. Int. Ed. Engl.*, 1995, **34**, 259–281.
146 R. A. Sheldon, *Pure Appl. Chem.*, 2000, **72**, 1233–1246.
147 D. J. C. Constable, A. D. Curzons and V. L. Cunningham, *Green Chem.*, 2002, **4**, 521–527.
148 R. A. Sheldon, *ACS Sustainable Chem. Eng.*, 2018, **6**, 32–48.
149 D. J. C. C. Alexei Lapkin, *Green Chemistry Metrics: Measuring and Monitoring Sustainable Processes*, Wiley-Blackwell, 2008.
150 J. Martínez, J. F. Cortés and R. Miranda, *Journal*, 2022, **10**(7), 1274.
151 S. Gülcemal, D. Gülcemal, G. F. Whitehead and J Xiao, Acceptorless Dehydrogenative Oxidation of Secondary Alcohols Catalysed by Cp*Ir(III) -NHC Complexes, *Chemistry*, 2016, **22**(30), 10513–10522.
152 S. Zhang, S. D. Foyle, A. Okrut, A. Solovoy, A. Katz, B. Gates and D. Dixon, Role of N-Heterocyclic Carbenes as Ligands in Iridium Carbonyl Clusters, *Phys. Chem. A*, 2017, **121**(26), 5029–5044.
153 F. T. Lapidoe, M. Kooti and J. S. Merola, Oxidative Addition of O-H Bonds to Iridium(I): Synthesis and Characterization of (Phenolato)- and (Carboxylato)iridium (III) Hydride Complexes, *Inorg. Chem*, 1993, **32**(9), 1681–1688.
154 A. Milet, A. Dedieu, G. Kapteijn and G. vanKoten, σ-Bond Metathesis Reactions Involving Palladium(II) Hydride and Methyl Complexes: A Theoretical Assessment, *Inorg. Chem*, 1997, **36**(15), 3223–3231.

